On the Optimization of Cyclic Adsorption Separation Processes

P. Cruz, F. D. Magalhães, and A. Mendes
Laboratory of Energy, Process, and Environmental Engineering (LEPAE), Depto. de Engenharia Química, Faculdade de Engenharia, Universidade do Porto, 4200-465 Porto, Portugal

DOI 10.1002/aic.10400
Published online March 25, 2005 in Wiley InterScience (www.interscience.wiley.com).

An innovative approach for the optimization of general cyclic adsorption separation processes (PSA and VSA), using the Skarstrom cycle with equalization, is proposed. The main objective is to study the optimal operating conditions for different adsorbent types, the optimal equalization stage configurations, and different underlying assumptions that are usually presumed in process modeling and simulation. The partial differential equations corresponding to the bulk gas-phase mass balances were solved with a recent numerical technique, developed within our group, based on an adaptive multiresolution approach. The partial differential equations for the intraparticle balances were solved using the orthogonal collocation method. The proposed dynamic simulator proved to be very efficient in terms of computational time and memory requirements: stability and accuracy are simultaneously ensured. The optimization was performed with a successive quadratic-programming algorithm that proved to be efficient because the optimum can be reached in a modest number of iterations. The proposed approach was applied to the particular case of oxygen production from air by PSA and VSA, with the aim of studying the performance of two commercially available adsorbents, commonly used in this specific separation, and the best configuration during equalization stage. © 2005 American Institute of Chemical Engineers *AIChE J,* 51: 1377–1395, 2005
Keywords: gas separation, adsorption, modeling, optimization, dynamic simulation

Introduction

In the last decades, the application of cyclic adsorption processes in gas separation increased significantly, fundamentally because of their performance with respect to both process economics and attainable product purity.[1]

These processes are based on the selective retention (based on adsorption equilibrium selectivity or diffusive selectivity) of one or more components in a gas mixture, with the adsorbent regeneration being performed by total or partial pressure decrease [pressure swing adsorption (PSA), vacuum swing adsorption (VSA), or vacuum pressure swing adsorption (VPSA)] or by temperature increase [temperature swing adsorption (TSA)]. The processes are intrinsically dynamic, operating in a periodic fashion with a fixed (or variable) time cycle.

This technology is nowadays very competitive, compared to other available technologies such as cryogenic distillation, as a result of the technological developments that brought many improvements over the original process, proposed in 1942 by Khale for air-drying.[2] Commercial acceptance has also been remarkable.[3-5]

The patents by Skarstrom[6] in 1960 and Montgareuil and Domine[7] in 1964 have decisively determined the technological development, leading in 1964 to the first practical implementation, for oxygen production from air. This was possible thanks to the development of synthetic zeolites,[8,9] with higher nitrogen/oxygen adsorption selectivity. Many improvements obtained in this field,[10-16] as well as the design of new cycle configurations and devices,[17,18] are the main reasons for the success of the technology.

Correspondence concerning this article should be addressed to A. Mendes at mendes@fe.up.pt.

The process developed by Skarstrom[6] has two columns (fixed beds) and works with a four-stage cycle: pressurization, production, depressurization, and purge. A great improvement over this process was the introduction of an equalization stage.[19-22] The pressure equalization leads to a substantial reduction in power consumption, given that less mechanical energy is required to pressurize the column that ended the purge stage. The product recovery is also increased because less feed/product ratio is necessary to pressurize the bed. The introduction of multiple columns, that is, in large-scale hydrogen production (normally between 10 to 12 beds), has also led to an improvement in process performance.[23-26] Processes with multiple columns have a higher number of pressure equalization stages, consequently reducing the amount of feed gas necessary for pressurization.[27] Other minor modifications have also been introduced: the stage of self-purging in kinetic-controlled separations,[28] layered beds,[29,30] and hybrid processes, involving materials such as membrane modules in combination with PSA.[31-35]

The process performance is substantially affected by a great number of design (bed size, adsorbent physical properties, configuration, and number of columns) and operating parameters (pressurization time, production time, desorption time, purge time, inlet flow rate, purge flow rate, production flow rate, pressure, and or temperature variations). Therefore, an optimization must be performed, which must take into account the initial investment, the operational costs, and the product sale profits. The objective function of the optimization problem, in large-scale production, should maximize the cumulative cash flow within the lifetime of the equipment.

In cyclic adsorption processes, the operational costs are associated with the maintenance, the energy, and the raw material, whereas the investment is related to the acquisition costs for adsorbent, columns, compressor, valves, sensors, and controllers. As in other process, the operational costs vary inversely with the recovery (defined as the ratio between produced and fed amounts of the desired component) and its reduction can be naturally obtained by an increase in the investment. For a predefined unit and for a desired product purity and flow rate, the optimization objective function corresponds to a maximization of the recovery, in that less energy is necessary to compress the gas (in PSA) and less raw material is used. If one performs some optimizations for different product flow rate values, the characteristic curve of the equipment can be plotted: as the product flow rate increases, both the recovery and the operational costs should decrease. The cumulative cash flow can be calculated for each product flow rate value and the optimum can be obtained.

This procedure is simple and straightforward to implement, although it is not convenient in terms of design, given that the design parameters (column length and diameter and the adsorbent type) are assumed a priori. Some relevant articles can be found in the literature presenting theoretical and experimental studies on this subject.[36-39]

A systematic theoretical optimization procedure, to determine the optimum design and operating conditions, however, is a difficult numerical task because it requires a high CPU time consumption, that is, when complex models are used to describe the process. The choice of the appropriate optimization variables may also be difficult. To overcome the first factor, Smith and Westerberg[40] used a very simple model to describe the cyclic adsorption process, considering simple time-integrated balances to describe the initial and final concentrations and temperature profiles for each process stage; however, the model considered a large number of optimization variables.

Nilchan and Pantelides[41] proposed a more general optimization procedure, focused on reducing the required power consumption. Two processes were considered: oxygen production from air using RPSA (rapid pressure swing adsorption) and nitrogen production from air using PSA. Unfortunately, the simulation results presented for both cases were restricted to a given product flow rate and to a column diameter and no attempt was made to study the influence of the product flow rate in the optimization performed. The authors discretized the model equations both in the temporal and spatial domains using finite-difference methods, obtaining a large set of algebraic equations. These equations, together with the periodic cyclic steady-state condition and control constraints, were solved using a nonlinear solver.

Ding et al.[42] proposed an alternative method for determining the optimum cyclic steady state (CSS). The authors applied their method to two different examples: single-bed PSA cycle for air purification and single-bed TSA for recovery of benzene and cyclohexane. In the first example they considered constant interstitial gas velocity, and so they assumed as objective function as the difference between the feed and purge velocities (which are directly related with the process recovery). In this example, however, no attempt was made to understand the influence of the cycle time. In the second example they considered local equilibrium between fluid and adsorbed phase and so the optimum is independent of the product flow rate. No attempt was made to understand the influence of the mass transfer resistance in the maximum product flow rate. In both examples the column's geometry was imposed a priori.

Jiang et al.[43] proposed an algorithm to accelerate the CSS convergence; they implemented a direct determination approach using a Newtonian-based method with accurate sensitivities to achieve fast and robust convergence. They applied their method to two different single-bed oxygen VSA cycles. In their first example they used a single-bed three-step oxygen VSA cycle. They assumed as constant the adsorption and desorption pressures. They chose to maximize oxygen recovery using as decision variables the tank pressure, the valve constant (from the bed to the tank), and the adsorption and desorption times. The column's geometry and product flow rate were imposed a priori. In the second example they used a more complex process: a single-bed six-step oxygen VSA cycle. In this example they chose to minimize the specific work while maintaining 95% oxygen purity using a predetermined column length. In this example, because no restrictions were made to the product flow rate, the optimization led to a pseudo-optimum solution because it does not depend on the product flow rate.

In these studies[41-43] some optimization algorithms were presented that can be straightforwardly used in optimization of cyclic adsorption processes. However, they do not provide a sufficiently general formulation: the design parameters (column's length and diameter and the adsorbent type) are assumed a priori, the product flow rate is normally assumed constant, and no attempt was made to understand the influence of the assumptions on the process simulation results.

To overcome these critical issues, Cruz et al.[44] proposed a

systematic theoretical optimization to design and optimize small- and large-scale units. This approach was applied to air separation by PSA and VSA using the classical Skarstrom cycle.[6] In this work, an extension of that technique is proposed, to optimize more complex cycles, analyze different types of adsorbents, and study some assumptions that are normally accepted when modeling cyclic adsorption processes.

An efficient and robust process simulator was developed. The system of partial differential equations in the bulk gas phase was solved using an adaptive multiresolution approach, ensuring great stability and accuracy of the simulated solution. The adaptive multiresolution approach is a recent numerical technique, developed within our group.[45] The system of partial differential equations, with respect to intraparticles, was solved using orthogonal collocation.[46] In terms of computational time, numerical stability, and accuracy, the adaptive multiresolution approach proved to be superior compared with other methods for the solution of the bulk gas-phase equations, that is, for conditions close to the equilibrium between fluid and adsorbed phase, when sharp concentrations fronts are formed.

The remainder of the article is organized as follows: first the mathematical model and the strategy adopted in the numerical solution are presented, as well as a small discussion on the implementation of nonlinear high-resolution schemes. Then the adopted optimization strategy and the algorithm used are described. Next, a performance analysis is presented for two different types of adsorbents using the Skarstrom cycle with equalization and some assumptions, usually made in cyclic adsorption processes modeling, are analyzed. The article ends with a summary of the main conclusions.

Mathematical Model

The theoretical model proposed considers a PSA/VSA system with two adsorbent beds having the same geometry, operating under the Skarstrom cycle with and without equalization steps. The following main assumptions are made: perfect gas behavior, axially dispersed plug flow, uniform cross-sectional void fraction, uniform adsorbent properties along the column, negligible radial gradients, and isotherm behavior. Figure 1 presents the basic process configuration (for the Skarstrom cycle).

According to these assumptions, the model equations can be written in dimensionless form as follows.[44]

Mass balance equations

Interparticle Total Mass balance

$$\frac{\partial p_T^*}{\partial \theta} = -\frac{\partial (u^* p_T^*)}{\partial x} - \sum_{i=1}^{nc} N_i^* \tag{1}$$

Interparticle Partial Mass Balance

$$\frac{\partial y_i}{\partial \theta} = \frac{1}{\mathrm{Pe}}\left(\frac{1}{p_T^*}\frac{\partial p_T^*}{\partial x}\frac{\partial y_i}{\partial x} + \frac{\partial^2 y_i}{\partial x^2}\right) - u^*\frac{\partial y_i}{\partial x} + \frac{1}{p_T^*}\left(y_i \sum_{j=1}^{nc} N_j^* - N_i^*\right) \tag{2}$$

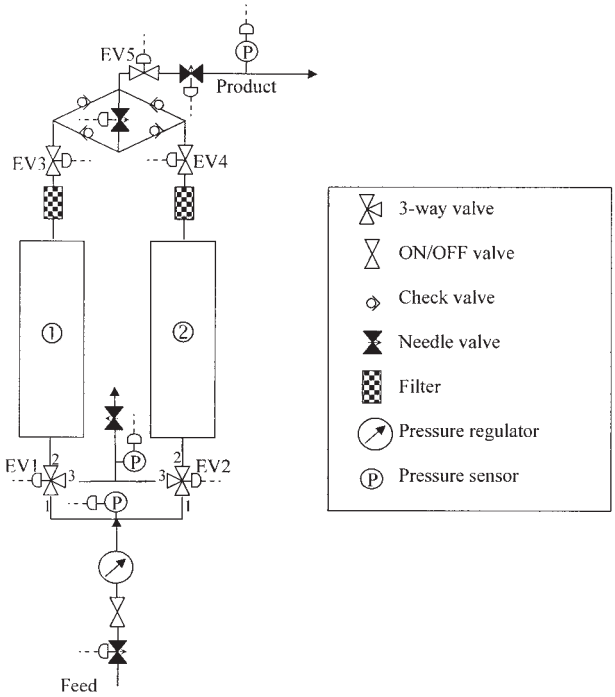

Figure 1. Sketch of PSA/VSA system implementing the Skarstrom cycle without equalization.

where p_T^* is the dimensionless total pressure; $p_T^* = p_T/p_{\mathrm{ref}}$; θ is the dimensionless time variable, $\theta = t/\tau_b$, where τ_b is the bed time constant, $\tau_b = L/u_{\mathrm{ref}}$; u^* is the average dimensionless molar velocity, $u^* = u/u_{\mathrm{ref}}$; x is the dimensionless axial coordinate, $x = z/L$; N_i^* is the ith component dimensionless molar flow rate, $N_i^* = N_i\tau_b/(\varepsilon_b c_{\mathrm{ref}})$; and Pe is the Peclet number, $\mathrm{Pe} = u_{\mathrm{ref}}L/D_{ax}$. The other symbols are referenced under Notation.

Pressure drop

In this work, as in our previous work,[44] we assumed negligible pressure drop and pressure drop described by the d'Arcy equation. The equations can be written in dimensionless form as follows.

No Pressure Drop

$$p_T^*(x) = \text{constant} \tag{3}$$

d'Arcy Equation

$$-\frac{\partial p_T^*}{\partial x} = \alpha u^* \tag{4}$$

where α is the dimensionless d'Arcy equation parameter.

$$\alpha = \frac{150\mu_{\mathrm{mix}}(1-\varepsilon_b)^2 u_{\mathrm{ref}} L}{\varepsilon_b^3 d_p^2 p_{\mathrm{ref}}} \tag{5}$$

Mass exchange rate

The mass exchange rate between the particle and its surroundings is given in dimensionless form by the following equation

$$N_i^* = \zeta_p \frac{\partial \bar{c}_i^*}{\partial \theta} + \zeta_a \frac{\partial \bar{q}_i^*}{\partial \theta} \tag{6}$$

where ζ_a is the adsorbed phase capacity factor, $\zeta_a = (1 - \varepsilon_b)/\varepsilon_b \rho_s q_{\text{ref}}/c_{\text{ref}}$ and ζ_p is the fluid phase capacity factor, $\zeta_p = (1 - \varepsilon_b)/\varepsilon_b \varepsilon_p$. ε_p is the particle porosity, $\bar{q}_i$ is the average molar concentration in the adsorbed phase, and $\bar{c}_i$ is the molar average concentration in the fluid phase.

Intraparticle mass transfer

To understand its influence in the simulation results, different approximations will be considered for describing the intraparticle mass transfer. The approximations considered are:

TM1. Linear driving force (LDF) approximation,[47] assuming as negligible the accumulation in the intraparticle (nonadsorbed) gas phase ($\partial \bar{c}_i/\partial \theta = 0$). This model can be derived from the intraparticle mass balance equation, which is a partial differential equation, considering parabolic profile inside the particle.[48] This assumption is valid only for long adsorption cycles. The same equation is obtained by applying the weighted residuals method with one point.[46]

$$\frac{d\bar{q}_i}{d\theta} = k_i(q_{i,s} - \bar{q}_i) \qquad \text{and} \qquad \frac{\partial \bar{c}_i}{\partial \theta} = 0 \tag{7}$$

where k_i is the LDF coefficient, $k_i = 15 D_{M,i}^e/r_p^2$, $D_{M,i}^e$ is the effective homogeneous diffusion coefficient, r_p is the particle radius, $q_{i,s}$ is the molar concentration in the particle surface (adsorbed phase) that is related with molar concentration in the interparticle gas phase through the adsorption equilibrium isotherm: $q_{i,s} = f(p_T, y_i)$. In dimensionless form

$$\frac{d\bar{q}_i^*}{d\theta} = \varphi \alpha_i^M (q_{i,s}^* - \bar{q}_i^*) \qquad \text{and} \qquad \frac{\partial \bar{c}_i^*}{\partial \theta} = 0 \tag{8}$$

where $\varphi = \tau_b k_{\text{ref}}$ and $\alpha_i^M = D_{M,i}^e/D_{\text{ref}} = k_i/k_{\text{ref}}$. The subscript "ref" means reference condition.

TM2. Linear driving force approximation,[47] assuming instantaneous equilibrium between the interparticle gas phase and the intraparticle gas phase ($\partial \bar{c}_i^*/\partial \theta = \partial c_i^*/\partial \theta$)

$$\frac{d\bar{q}_i^*}{d\theta} = \varphi \alpha_i^M (q_{i,s}^* - \bar{q}_i^*) \qquad \text{and} \qquad \frac{\partial \bar{c}_i^*}{\partial \theta} = \frac{\partial c_i^*}{\partial \theta} \tag{9}$$

TM3. Linear driving force dusty-gas approximation (LDF-DG)

$$\begin{aligned}\left[\varepsilon_p \mathbf{I} + \rho_s \frac{p_{\text{ref}}}{c_{\text{ref}}} \mathbf{J}\right] \frac{\partial \bar{\mathbf{p}}^*}{\partial \theta} &= \varphi \varepsilon_p \mathbf{B}^{-1}[(\mathbf{p}^*)_{R=1} - \bar{\mathbf{p}}^*] \\ &+ \varphi \varepsilon_p \mathbf{\Lambda}\{[(p_T^*)_{R=1} - \bar{p}_T^*]\bar{\mathbf{p}}^* + [(p_T^*)_{R=1} - \bar{p}_T^*][(\mathbf{p}^*)_{R=1} - \bar{\mathbf{p}}^*]\} \\ &+ \varphi \varepsilon_p \mathbf{B}^{-1}\mathbf{C}\mathbf{B}^{-1}\{[(\mathbf{p}^*)_{R=1} - \bar{\mathbf{p}}^*] + \mathbf{\Lambda}[(p_T^*)_{R=1} - \bar{p}_T^*]\bar{\mathbf{p}}^*\}\end{aligned} \tag{10}$$

where $\mathbf{J}$ is the Jacobian matrix of the adsorbed concentration to the partial pressure, $\mathbf{I}$ is the identity matrix, $\mathbf{B}$ is the diffusivity matrix in the dusty-gas model, $\mathbf{\Lambda}$ is the pressure drop parameter, and $\mathbf{C}$ is the derivative of the diffusivity matrix. This approximation can be derived from the dusty-gas model[49] using the orthogonal collocation method with one collocation point.

TM4. Homogeneous mass diffusion equation, assuming instantaneous equilibrium in the intraparticle gas phase ($\partial \bar{c}_i^*/\partial \theta = \partial c_i^*/\partial \theta$)

$$\frac{\partial q_i^*}{\partial \theta} = \Phi \frac{1}{R^2} \frac{\partial}{\partial R}\left(R^2 \alpha_i^M \frac{\partial q_i^*}{\partial R}\right) \qquad \text{and} \qquad \frac{\partial \bar{c}_i^*}{\partial \theta} = \frac{\partial c_i^*}{\partial \theta} \tag{11}$$

where $\Phi = \tau_b D_{\text{ref}}/r_p^2$ and R is the dimensionless radial coordinate.

TM5. Dusty-gas model[49]

$$\left(\varepsilon_p \mathbf{I} + \rho_s \frac{q_{\text{ref}}}{c_{\text{ref}}} \mathbf{J}\right) \frac{\partial \mathbf{p}^*}{\partial \theta} = -\frac{\Phi}{R^2} \frac{\partial}{\partial R}\left[R^2\left(\varepsilon_p \mathbf{N}^{p*} + \rho_s \frac{q_{\text{ref}}}{c_{\text{ref}}} \mathbf{N}^{s*}\right)\right] \tag{12}$$

where $\mathbf{p}$ is the partial pressure vector of nc components in the void space, $\mathbf{q}$ is the concentration vector in the adsorbed phase, and ρ_s is the apparent particle density. Vectors $\mathbf{N}^p$ and $\mathbf{N}^s$ are the fluxes in the void space and in the adsorbed phase, respectively.

The TM1, TM2, and TM3 are based on linear driving force approximation. These approximations are described by an ordinary differential equation for each component. TM4 and TM5—approximations that result from the application of mass balances to the particle—are described by a system of partial differential equations. The application of these models in the simulation of cyclic adsorption processes, coupled with mass balance equations for the bulk gas phase, results in a problem with two different space regions: bulk gas phase and particle phase.

Approximations TM4 and TM5 were solved using orthogonal collocation. In the case of homogeneous diffusion equation, the orthogonal collocation method can be applied straightforwardly,[46] if one assumes a polynomial approach for q_i^* of the following form

$$q_i^* = q_{i,s}^* + \sum_{j=1}^{n} a_{i,j}(R^{2j} - 1) \tag{13}$$

For $n = 2$, the following system of ordinary differential equations is obtained (for detailed derivation see Cruz et al.[46])

$$\begin{aligned}\frac{dq_{i,1}^*}{d\theta} &= \varphi \alpha_i^M(-28.167 q_{i,1}^* + 35\bar{q}_i^* - 6.833 q_{i,s}^*) \\ \frac{d\bar{q}_i^*}{d\theta} &= \varphi \alpha_i^M(34.833 q_{i,1}^* - 76.833\bar{q}_i^* + 42 q_{i,s}^*)\end{aligned} \tag{14}$$

For $n = 3$, the following system of ordinary differential equations is obtained

$$\frac{dq^*_{i,1}}{d\theta} = \varphi\alpha_i^M(-13.247q^*_{i,1} + 43.179q^*_{i,2} - 35.928\bar{q}^*_i + 5.996q^*_{i,s})$$

$$\frac{dq^*_{i,2}}{d\theta} = \varphi\alpha_i^M(-17.025q^*_{i,1} - 113.156q^*_{i,2} + 147.889\bar{q}^*_i - 17.709q^*_{i,s})$$

$$\frac{d\bar{q}^*_i}{d\theta} = \varphi\alpha_i^M(46.339q^*_{i,1} + 124.259q^*_{i,2} - 251.597\bar{q}^*_i + 81q^*_{i,s}) \quad (15)$$

Moreover, Cruz et al.[46] demonstrated than these approximations are mathematically identical to those derived by Lee and Kim,[50] from the analytical solution of the mass balance equation in the Laplace domain.

Boundary conditions

Stage One (Pressurization/Despressurization Stage). The boundary equations can be written in dimensionless form as follows[44]:

- Column (1)

$$x = 0 : p^*_T = f^*_p(\theta_c) \qquad \frac{1}{\mathrm{Pe}}\frac{\partial y_i}{\partial x} = u^*(y_i - y_{\mathrm{in},i})$$

$$x = 1 : u^* = 0 \qquad \frac{\partial y_i}{\partial x} = 0$$

- Column (2)

$$x = 0 : p^*_T = f^*_d(\theta_c) \qquad \frac{\partial y_i}{\partial x} = 0$$

$$x = 1 : u^* = 0 \qquad \frac{\partial y_i}{\partial x} = 0$$

where

$$f^*_p(\theta_c) = \frac{f_p(\theta_c\tau_b)}{p_{\mathrm{ref}}} \qquad \text{and} \qquad f^*_d(\theta_c) = \frac{f_d(\theta_c\tau_b)}{p_{\mathrm{ref}}}$$

and $f^*_p(t_c)$ and $f^*_d(t_c)$ are arbitrary functions that describe the total pressure variation as a function of time in each column, during the pressurization and depressurization stages, respectively. In this work we use the following functions

$$f^*_p(\theta_c) = p^{L*}_T + \frac{1 - \exp[-\theta_c/(a\theta_{\mathrm{pres}})]}{1 - \exp(-1/a)}(p^{H*}_T - p^{L*}_T) \quad (16)$$

$$f^*_d(\theta_c) = p^{H*}_T - \frac{1 - \exp[-\theta_c/(a\theta_{\mathrm{pres}})]}{1 - \exp(-1/a)}(p^{H*}_T - p^{L*}_T) \quad (17)$$

The symbols are described under Notation. These empirical expressions are almost general, reducing to linear relations (Eqs. 18 and 19 below) when $a \to \infty$ and instantaneous pressurization when $a \to 0^+$.

$$f^*_p(\theta_c) = p^{L*}_T + (\theta_c/\theta_{\mathrm{pres}})(p^{H*}_T - p^{L*}_T) \quad (18)$$

$$f^*_d(\theta_c) = p^{H*}_T - (\theta_c/\theta_{\mathrm{pres}})(p^{H*}_T - p^{L*}_T) \quad (19)$$

where $p^{H*}_T = p^H_T/p_{\mathrm{ref}}$, $p^{L*}_T = p^L_T/p_{\mathrm{ref}}$, $\theta_{\mathrm{pres}} = t_{\mathrm{pres}}/\tau_b$, and $\theta_c = t_c/\tau_b$.

Some trial work was previously carried out to determine the influence of the empirical parameter a. The optimization results indicate that the maximum recovery is directly related with this parameter, although its influence is practically negligible for $a \geq 0.1$. The results presented in this work are for $a \to \infty$.

Stage 2 (Production/Purge Stage). The boundary equations can be written in dimensionless form as follows[44]

- Column (1)

$$x = 0 : p^*_T = p^{H*}_T \qquad \frac{1}{\mathrm{Pe}}\frac{\partial y_i}{\partial x} = u^*(y_i - y_{\mathrm{in},i})$$

$$x = 1 : u^* = u^*_{\mathrm{prod}} \qquad \frac{\partial y_i}{\partial x} = 0$$

- Column (2)

$$x = 0 : p^*_T = p^{L*}_T \qquad \frac{\partial y_i}{\partial x} = 0$$

$$x = 1 : u^* = \chi\frac{p^H_T}{p^L_T} \qquad \frac{1}{\mathrm{Pe}}\frac{\partial y_i}{\partial x} = u^*(y_i - y_i|_{x=1})$$

where u_{prod} and u_{purg} are the production and purge velocities, respectively; χ is the normalize purge flow, $\chi = (u_{\mathrm{purg}}/u_{\mathrm{ref}})(p^L_T/p^H_T)$. The other symbols are described under Notation.

Stage 3 (Equalization Stage). The equalization stage[19-22] was a very important improvement introduced in these processes. The pressure equalization, using a product-enriched current, leads to a significant economy in power consumption, given that less mechanical energy is required to repressurize the column that is at low pressure, at the end of the purge stage. In this way, the product recovery is also increased because less feed gas is necessary to repressurize the column. The boundary conditions for the three configurations studied in this work (Figure 2) are presented next in dimensionless form

(1) Configuration M1—Top to bottom

- Column (1)

$$x = 0 : u^* = 0 \qquad \frac{\partial y_i}{\partial x} = 0$$

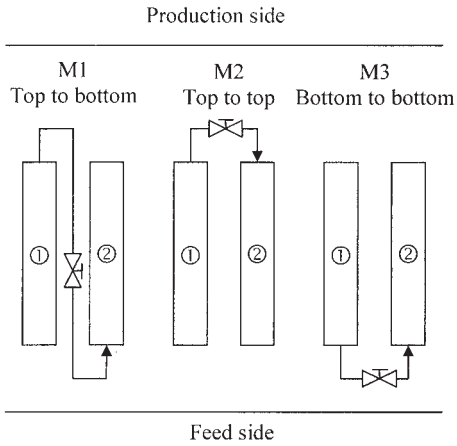

Figure 2. Three different configurations during the equalization stage.

$$x = 1 : u^* \text{ given by valve equation:} \qquad \frac{\partial y_i}{\partial x} = 0$$

- Column (2)

$$x = 0 : u^* \text{ given by valve equation:} \qquad \frac{1}{\text{Pe}}\frac{\partial y_i}{\partial x} = u^*(y_i - y_i|_{x=1}^{\text{column(1)}})$$

$$x = 1 : u^* = 0 \qquad \frac{\partial y_i}{\partial x} = 0$$

Valve equations

- EV1—Chou and Huang[51,52]

$$u^* p_T^* = \begin{cases} 1.179\phi\sqrt{(p_T^*|_{i\text{col}=1})^2 - (p_T^*|_{i\text{col}=2})^2} \\ \quad \text{when } p_T^*|_{i\text{col}=2} > 0.528 p_T^*|_{i\text{col}=1} \\ \phi p_T^*|_{i\text{col}=1} \\ \quad \text{when } p_T^*|_{i\text{col}=2} \le 0.528 p_T^*|_{i\text{col}=1} \end{cases}$$

- EV2—Linear valve

$$u^* p_T^* = \phi(p_T^*|_{i\text{col}=1} - p_T^*|_{i\text{col}=2})$$

where ϕ is the valve dimensionless coefficient.

(2) Configuration M2—Top to top

- Column (1)

$$x = 0 : u^* = 0 \qquad \frac{\partial y_i}{\partial x} = 0$$

$$x = 1 : u^* \text{ given by valve equation:} \qquad \frac{\partial y_i}{\partial x} = 0$$

- Column (2)

$$x = 0 : u^* = 0 \qquad \frac{\partial y_i}{\partial x} = 0$$

$$x = 1 : u^* \text{ given by valve equation:} \qquad \frac{1}{\text{Pe}}\frac{\partial y_i}{\partial x} = u^*(y_i - y_i|_{x=1}^{\text{column(1)}})$$

(3) Configuration M3—Bottom to bottom

- Column (1)

$$x = 0 : u^* \text{ given by valve equation:} \qquad \frac{\partial y_i}{\partial x} = 0$$

$$x = 1 : u^* = 0 \qquad \frac{\partial y_i}{\partial x} = 0$$

- Column (2)

$$x = 0 : u^* \text{ given by valve equation:} \qquad \frac{1}{\text{Pe}}\frac{\partial y_i}{\partial x} = u^*(y_i - y_i|_{x=0}^{\text{column(1)}})$$

$$x = 1 : u^* = 0 \qquad \frac{\partial y_i}{\partial x} = 0$$

Adsorption equilibrium

In this work, the Langmuir–Freundlich isotherm and the ideal adsorption solution theory (IAST[53]) are used to describe the multicomponent equilibrium.

Langmuir–Freundlich Isotherm

$$q_i = \frac{q_{\max,i}(b_i p_i)^{1/n_i}}{1 + \sum (b_i p_i)^{1/n_i}} \tag{20}$$

The IAST algorithm is described in Myers and Prausnitz.[53] The monocomponent isotherm used in the IAST algorithm was the Langmuir–Freundlich.

Model Numerical Solution

The model developed is defined by a system of partial differential equations (mass balances in the bulk gas phase and in the particle), coupled with a system of ordinary differential equations (linear driving force–based approximations). In the case of using the mass balance in the particle, the model is defined in two different regions: bulk gas phase and particle.

The partial differential equations from the mass balance in the bulk gas phase are parabolic equations, in which the convective term predominates over the diffusive term. The diffusive term, as will be seen in this work, is almost negligible for Peclet numbers > 600. The partial differential equations from mass balance in the particle are also parabolic equations, although these are controlled by diffusion (in the case of homogeneous diffusion equation, only the diffusive term exists, whereas the dusty-gas model has both a diffusive and a convective term).

To solve the model efficiently, it is important to use specific methods for the two types of equations. In a previous work,[45] we showed that the application of high-order discretization schemes to the resolution of hyperbolic and/or parabolic equations dominated by advection leads to the appearance of oscillations without physical meaning in the solution, which, in the case of hyperbolic equations, do not disappear with mesh refinement. For these cases, the use of nonlinear high-resolution schemes was suggested, which proved to avoid these problems. The use of an adaptive multiresolution approach for this type of equations was also proposed[45] and is the method used in this work.

In previous works, we have shown that the orthogonal collocation method is the best numerical tool for the solution of parabolic equations dominated by diffusion. This method allows us to obtain—for the case of homogeneous diffusion—expressions that are equivalent to those derived from the analytical solution.[46]

Discretization of the model's partial differential equations is done in two stages. First, the space derivatives are computed using appropriate schemes. Then, the resulting initial value system of ordinary differential equations is integrated explicitly to obtain the grid point values at the next time step. This time integration is done using the package LSODA.[54]

In the simulator developed for this work, the convective terms from mass balance equations in the bulk gas phase are discretized using nonlinear high-resolution schemes and the diffusive terms are discretized using central finite differences. The mass balance equations in the particle are discretized using orthogonal collocation. The efficiency of the simulator is substantially improved by the introduction of the adaptive multiresolution approach. The simulator proved to be very efficient with respect to computational time, numerical stability, and accuracy.

Nonlinear High-Resolution Schemes

As mentioned earlier, the application of conventional higher-order discretization schemes to the advective term (convection term) of hyperbolic or parabolic equations dominated by diffusion is not adequate because of the occurrence of nonphysical oscillations.

To overcome this issue, an extensive amount of research has been directed toward the development of accurate and bounded nonlinear convective schemes. Several discretization schemes were proposed on the total variation-diminishing framework (TVD)[55,56] and, more recently, on the normalized variable formulation (NVF)[57] and its extension, the normalized variable and space formulation (NVSF) of Darwish and Moukalled.[58] The high-resolution schemes implemented in this work for the discretization of the problematic convection term are based on this last formulation.

The flux derivative at the general point i is evaluated from the following expression

$$\left.\frac{\partial F}{\partial x}\right|_i = \frac{(F_{i+1/2} - F_i)(x_i - x_{i-1})^2 + (F_i - F_{i-1/2})(x_{i+1} - x_i)^2}{(x_i - x_{i-1})(x_{i+1} - x_i)(x_{i+1} - x_{i-1})/2} \tag{21}$$

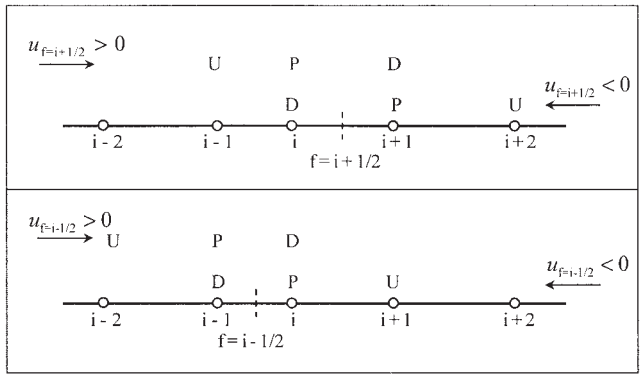

Figure 3. Definition of local variables.

where the unknown face fluxes $F_{i+1/2}$ and $F_{i-1/2}$ are interpolated from the neighbor grid point values using an appropriate discretization scheme.

Consider a general nonuniform grid, as illustrated in Figure 3. The labeling of the nodes depends on the local velocity. For a given face f, the U and D nodes refer to the upstream and downstream points, relative to node P, which is itself upstream to the face f under consideration, as shown in Figure 3.

According to the NVSF, the face fluxes are interpolated as[58]

$$F_f = F_U + \hat{F}_f(F_D - F_U) \tag{22}$$

where the normalized face flux, $\hat{F}_f$, is calculated using an appropriate nonlinear limiter. In this work, the SMART limiter was used[59]

$$\hat{F}_f = \max\left[\hat{F}_P, \min\left(\frac{\hat{x}_f(1 - 3\hat{x}_P + 2\hat{x}_f)}{\hat{x}_P(1 - \hat{x}_P)}\hat{F}_P, \frac{\hat{x}_f(1 - \hat{x}_f)}{\hat{x}_P(1 - \hat{x}_P)}\hat{F}_P + \frac{\hat{x}_f(\hat{x}_f - \hat{x}_P)}{1 - \hat{x}_P}, 1\right)\right] \tag{23}$$

where the normalized variables $\hat{F}_P$, $\hat{x}_P$, and $\hat{x}_f$ are calculated using

$$\hat{F}_P = \frac{F_P - F_U}{F_D - F_U} \qquad \hat{x}_P = \frac{x_P - x_U}{x_D - x_U} \qquad \hat{x}_f = \frac{x_f - x_U}{x_D - x_U} \tag{24}$$

More details on this issue, and other high-resolution schemes, can be found in the works of Darwish and Moukalled[58] and Alves et al.[60]

For uniform meshes, the normalized space coordinates defined in Eq. 24 are simply $\hat{x}_P = 1/2$ and $\hat{x}_f = 3/4$, and the limiter function (Eq. 23) is greatly simplified

$$\hat{F}_f = \max\left[\hat{F}_p, \min(3\hat{F}_P, \frac{3}{4}\hat{F}_P + \frac{3}{8}, 1)\right] \tag{25}$$

Optimization Strategy

As discussed earlier in the introduction, the performance of cyclic adsorption separation processes is substantially affected

Table 1. Reference Variables in the Model

Reference pressure: p_{ref} (Pa)	$p_{ref} = p_T^H$
Reference temperature, T_{ref} (K)	$T_{ref} = 293.15$
Reference concentration: c_{ref} (mol/m^3)	$c_{ref} = p_{ref}/(\Re T_{ref})$
Reference fluid velocity: u_{ref} (m/s)	$u_{ref} = u_{prod}$
Reference adsorbed phase concentration: q_{ref} (mol/kg)	$q_{ref} = q_{Nitrogen}(T_{ref}, p_{ref})$

by a large number of design variables (bed size, adsorbent physical properties, configuration, and number of columns) and operating variables (pressurization time, production time, desorption time, purge time, inlet flow rate, purge flow rate, production flow rate, and pressure and/or temperature variations). An optimization procedure considering all the above variables is a difficult numerical task, in that the number of optimization variables is extremely high and some of them are intrinsically related in a complex manner. To overcome this problem, Cruz et al.[44] proposed a systematic optimization approach, in dimensionless form, to design and optimize PSA/VSA units using the Skarstrom cycle. This work follows the same strategy, now applied to the study of more complex cycles, the analysis of different adsorbents for a given separation, and the discussion of the validity of normally accepted assumptions.

The basic idea behind this strategy is that, when the model equations are written in dimensionless form, the number of variables in the mathematical equations is reduced to a set of dimensionless variables that can be more simply optimized and whose influence on the process is easier to understand.

An important aspect in this procedure is the choice of the model's reference variables (variables used to dimensionalize the model equations). The reference component should be the most adsorbed. Considering the production of oxygen, this component is nitrogen. Table 1 lists the reference variables adopted here.

The optimization of cyclic adsorption processes must take into account the operating costs, the investment, and the product sales profits. Cruz et al.[44] showed that the objective function, assuming 0% amortization rate, can be written as follows

$$\hat{F}_{obj} = \left[1 - \frac{1}{\mathrm{Rec}}\frac{\mathrm{Pur}}{y_{in}}(W \cdot \$\mathrm{EC} + \$\mathrm{RC})\right] LT - \Omega^{-1}(\$\mathrm{C}_{ads} + (p_T^H)^{\beta} \cdot \$\mathrm{C}_{col}) - \frac{\kappa_1}{(Q_{prod})^{1-\gamma_1}}\left(\frac{1}{\mathrm{Rec}}\frac{\mathrm{Pur}}{y_{in}}\right)^{\gamma_1} - \frac{\kappa_2}{(Q_{prod})^{1-\gamma_2}}\left(\frac{1}{\mathrm{Rec}}\frac{\mathrm{Pur}}{y_{in}}W\right)^{\gamma_2} - \frac{\kappa_3}{(Q_{prod})^{1-\gamma_3}}\left(\frac{1}{\mathrm{Rec}}\frac{\mathrm{Pur}}{y_{in}}\right)^{\gamma_3} \quad (26)$$

where Pur is the product purity, Rec is the product recovery, W is the theoretical work (J/m$^3_{STP}$), Q_{prod} is the average product flow rate, \$EC is the energy cost (\$/J), \$RC is the raw material costs (\$/m$^3_{STP}$), LT is the lifetime of equipment (year), Ω is the adsorbent productivity (m$^3_{STP}$ year^{-1} m^{-3}), $\$C_{ads}$ is the cost of the adsorbent (\$/m^3), $\$C_{col}$ is the column cost, and β, κ_i, and γ_i are parameters of correlations,[61] to estimate the price of the compressor and other equipment, such as valves, sensors, and controllers.

In the objective function, the adsorbent productivity Ω can be related to parameter φ that appears in the dimensionless model equations, as follows

$$\Omega^{-1} = \frac{V}{Q_{prod}} = \frac{\mathrm{UC}}{k_{ref}}\frac{\Psi}{(1-\chi)} \quad \text{with} \quad \Psi = \varphi\frac{\theta_{prod} + \theta_{pres} + \theta_{equ}}{\theta_{prod}}\frac{p_{STP}}{p_T^H}\frac{T}{T_{STP}} \quad (27)$$

where UC is a units conversion factor and the subscript STP means standard temperature and pressure conditions. The objective function (Eq. 26) takes into account five fundamental quantities that can characterize the process: purity, recovery, adsorbent productivity, compressor work, and average product flow rate.

The dependency of the product flow rate is directly related with the unit scale factor. For high production levels, the terms that depend on Q_{prod} become negligible; however, for low production, they gain a considerable weight.

Two aspects stand out from the analysis of the objective function. First, all the terms are related with the recovery, with the exception of the adsorbent and column costs. Second, for a given operating pressure (that is, the work W is constant) and adsorbent productivity (Ω), the objective function increases with increasing recovery.

This analysis shows that for an already implemented unit, assuming a minimum flow rate, product purity, and a production pressure, the best performance is obtained for maximum recovery. However, if the raw material costs are zero then, for a minimum flow rate, the best performance corresponds to minimum power consumption. This implies that, in the optimization of cyclic adsorption processes, if the investment is negligible, compared with the operating costs and simultaneously the raw material, is costless (as is the case of oxygen production at large scale), the optimization strategy could be implemented to reduce the power consumption, assuming a minimum product flow rate per column volume (adsorbent productivity). However, if the investment is not negligible and/or the raw material is not costless, the optimization should be implemented to maximize the recovery for different pressure ratios and for different values of adsorbent productivity.[44] The optimum adsorbent productivity in the second approach can be obtained from the characteristic curve of the process (investment and operating costs as a function of the adsorbent productivity). This is the strategy adopted in this work.

The model equations for the cycle with equalization, in dimensionless form, present five decision variables in the second approach (maximization of the recovery): the normalized purge flow rate χ, the valve dimensionless coefficient ϕ, and three variables related with the cycle time (θ_{pres}, θ_{prod}, and θ_{equ}). In the first approach (minimization of power consumption) there is more one variable: the pressure ratio, p_T^H/p_T^L. Table 2 provides a summary of the optimization variables and their respective bounds.

The other dimensionless variables in the model are related to adsorbent data, flow pattern (Peclet number), and pressure drop. The parameter that characterizes the flow dispersion—the Peclet number—can be estimated assuming an average molar velocity, the components in the gas mixture, the particle diameter, and the column length.[3] For small-scale units, the values

Table 2. Optimization Variables with Their Respective Bounds

Maximization of Recovery			Minimization of Power Consumption		
Variable	Lower Bound	Upper Bound	Variable	Lower Bound	Upper Bound
θ_{pres}	0.1	10	θ_{pres}	0.1	10
θ_{prod}	0.1	10	θ_{prod}	0.1	10
θ_{equ}	0.1	10	θ_{equ}	0.1	10
χ	0	1	χ	0	1
ϕ	0.1	100	ϕ	0.1	100
			p_T^H/p_T^L	1	10

predicted are around 500 to 1000. The predicted performance of cyclic adsorption processes seem to be almost independent of its value when it is >600, as will be seen in this work.

The dimensionless treatment of the problem leads to decision variables with more restrictive variation ranges: the normalized production time varies between zero (no adsorbent utilization) and ζ_a (effective adsorbent utilization); the normalized purge flow rate varies between zero (no purge) and one (all product flow rate is used to clean the other column); the dimensionless pressurization time and the dimensionless equalization time should be of the same order as the dimensionless production time.

Optimization Algorithm

There are three different problems that occur in the optimization of cyclic adsorption processes. The first is related to the intrinsically dynamic nature of the problem. A cyclic adsorption processes does not have steady state because it always works in a dynamic fashion; only a cyclic steady state (CSS) can be defined.

The calculation of the CSS is one of the most challenging tasks in process control and optimization. Different strategies have been proposed recently to overcome this problem.[41-43] However, we do not find any of these advantageous with respect to the successive substitution method adopted here: when the CSS calculation is started from the previous one, the number of cycles necessary to reach the cyclic steady state is always <10. The strategy followed considers the simultaneous simulation of the two columns; this particular approach substantially reduces the number of cycles needed to reach the CSS. In this work we considered that the CSS was reached when the purity and recovery did no change more than 0.01%, absolute, in two consecutive cycles. Moreover, the purity and recovery used are extrapolated from the two last-computed cycles.

The error introduced in the solution by the simultaneous spatial and temporal discretization is the second problem. This issue does not have an equivalent in steady-state problems because there is no time dependency in these problems. In cyclic adsorption processes, the coupled error in space and time discretization leads to an unpredicted error, although this can be minimized by the use of efficient and robust numerical tools for space and time discretization.

In this work, the numerical error in space discretization is diminished by the use of high-resolution schemes in a very refined mesh and using a grid-adaptation strategy developed for the solution of hyperbolic equations.[45] The high-resolution schemes are intrinsically bounded, always leading to stable solutions, without physically meaningless oscillations. This aspect is also important when calculating the adsorption equilibrium, where negative concentrations lead to a mathematical impossibility. The error in temporal integration is minimized by the use of subroutine LSODA.[54] This subroutine has the advantage of being very versatile, changing automatically between methods for stiff and nonstiff initial value problems. In both methods the integration step and integration order are variable, thus minimizing the time integration error.

The third problem is the time necessary to compute the objective function. With our simulator, the calculation of the objective function takes about 10–20 s (1–2 s per cycle) in a Pentium IV 1.5-GHz personal computer. Therefore, for an efficient optimization, it is important to find the optimum within a moderate number of function evaluations.

To develop an efficient and robust algorithm to optimize cyclic adsorption processes, it is important to take into account these three issues: the error in the solution arising from the dynamic nature of the problem and from the temporal/spatial discretization and the time necessary to compute the objective function.

In this work, as in our previous work,[44] a successive quadratic-programming algorithm (SQP)[62] was used. This type of algorithm has the advantage of finding the optimum (local) with a limited number of function evaluations, as long as the estimate is close enough to the optimum and the objective function and the gradients (evaluated analytically or using finite differences) are evaluated with high precision.

Herein the gradients of objective function and constraint were calculated using forward finite differences, which means that for n optimization variables, there are $2n$ function calls. The SQP algorithm developed is briefly described in the Appendix.

Case Study: Production of Oxygen from Air

The simulations were performed for the production of oxygen from air (nitrogen, 78%; oxygen, 21%; argon, 1%) using both PSA and VSA. Three possible configurations during the equalization stage and two commercially available adsorbents (OXYSIV 5 and OXYSIV 7 UOP™, UOP LLC, Des Plaines, IL) were studied.

The single-component adsorption equilibrium isotherms were obtained experimentally by the volumetric method, using a setup developed in house[63] and confirmed by the gravimetric method using a Rubotherm magnetic suspension microbalance.[64] The results obtained by the two methods are in good agreement. The Langmuir–Freundlich isotherm parameters are presented in Table 3.

Because the adsorption equilibrium isotherms of oxygen and

Table 3. Single-Component Langmuir–Freundlich Isotherm Parameters

	OXYSIV 5 UOP™ *			OXYSIV 7 UOP™ *		
	$q_{max,i}$ (mol/kg)	b_i (bar^{-1}) at 20°C	n	$q_{max,i}$ (mol/kg)	b_i (bar^{-1}) at 20°C	n
N_2	2.996	0.105	1.0	3.90	0.0780	1.3
O_2 and Ar	4.875	0.022	1.0	4.43	0.0261	1.0

*OXYSIS 5 and OXYSIS 7 are trademarked proprietary products of UOP LLC, Des Plaines, IL.

argon are almost identical, it was decided to consider a pseudo binary mixture of nitrogen (78%) and oxygen (22%).

Optimization Results

The optimization results are presented and discussed in this section. First, different mass transport approximations are compared, to understand the differences between them and to select an approximation for the subsequent simulations that is simple but consistent. This analysis is performed considering the Skarstrom cycle and the adsorption equilibrium data of OXYSIV 5. The influence of pressure ratio (p_T^H/p_T^L), required purity, and inside bed temperature on the process performance (recovery and power consumption) are subsequently analyzed. Finally, the results for the Skarstrom cycle with equalization are presented, where the process performance is analyzed for the three configurations discussed earlier.

Analysis of intraparticle mass transfer approximations

This section deals with the comparison between the different intraparticle mass transfer approximations. The analysis is performed using the Skarstrom cycle, with the adsorption equilibrium data of adsorbent OXYSIV 5 for two pressure ratios: $p_T^H/p_T^L = 5$ and $p_T^H/p_T^L = 3$.

The approximations TM1, TM2, and TM3 are based on the linear driving force. TM1, which considers only accumulation in the adsorbed phase, is the most commonly used approximation. TM2 considers instantaneous equilibrium between the interparticle fluid phase and intraparticle fluid phase, which constitutes the only difference between TM1 and TM2.

TM3 (LDF-DG) is derived from the dusty-gas model, assuming a parabolic profile inside the particle. This approximation is included in our optimization procedure to understand the differences between the LDF approximation[47] (which is deduced assuming the validity of the Fick's law) and the dusty-gas model. A particle porosity of $\varepsilon_p = 0.33$ (determined by mercury porosimetry) is used in approximations TM2, TM3, and TM4.

TM4 is the mass diffusion model (or homogeneous diffusion model), assuming instantaneous equilibrium between the interparticle fluid phase and the intraparticle fluid phase. The partial differential equation was solved using orthogonal collocation.[45] Two, three, and four collocation points were used, without any significant difference between the results. The resolution of TM4, compared with the LDF approximation, is aimed at understanding the commonly discussed problems that arise from using the LDF approximation[45] in the simulation of cyclic adsorption processes.

Figure 4 shows the simulated results for a required purity of 95% as a function of Ψ (this variable behaves inversely with the adsorbent productivity; see Eq. 27). The reference diffusion

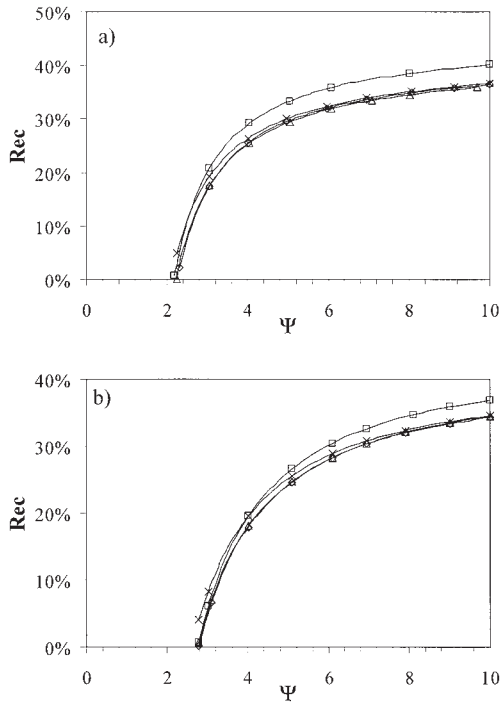

Figure 4. Maximum recovery as a function of Ψ for a required purity of 95% (O_2 + Ar) and high pressure.

(a) 5 bar and (b) 3 bar (PSA operation at 20°C). —□—, TM1; —◇—, TM2; —△—, TM3; —×—, TM4. The symbols presented are just to identify the curves.

coefficient used in TM3 was calculated at 3.7 bar, when the maximum pressure was 5 bar, and 2.3 bar, when the maximum pressure was 3 bar.

Approximations TM2, TM3, and TM4 present almost identical simulation results for the entire range of Ψ and all pressure ratios analyzed. Small differences are observed only between TM4 and the approximations TM2 and TM3 for small Ψ values. Small Ψ values are related to short cycles (maximum adsorbent productivity) and so the equilibrium between the fluid phase and adsorbed phase is less efficient.

The most important differences are obtained when comparing approximation TM1 with the others, that is, for high Ψ values. Approximation TM1 neglects accumulation in the intraparticle fluid phase. This assumption is normally accepted in cyclic adsorption processes simulation, although it leads to very different results from those of simulations that assume instantaneous equilibrium for the intraparticle fluid phase or using the dusty-gas model. The assumption of negligible accumulation in intraparticle fluid phase leads to higher values of

Table 4. Particle Porosity Values for Zeolites of Types 5A and 13X and Mass Transport Approximations Used

Reference	Zeolite Type	ε_p	Model
Farroq et al., 1989	5A	—	TM1
Liow and Kenney, 1990	5A	0.29	TM2
Mendes, 1993	5A	0.31	LDF-DG
Jee et al., 2001	5A	0.65	TM1*
Da Silva et al., 1999	13X	0.27	TM2*
Teague and Edgar, 1999	13X	0.53	TM1
Arwind et al., 2002	13X	0.28	TM1
Bitzer and Zeitz, 2002	13X	0.60	TM1

*Means that this reference is not related with oxygen production.

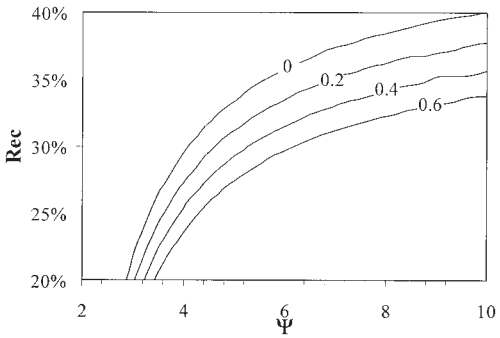

Figure 5. Maximum recovery as a function of Ψ value for a required purity of 95% (O_2 + Ar) and maximum pressure of 5 bar (PSA operation at 20°C).

Analysis for different particle porosity values (ε_p) (porosity of 0 is related to the use of TM1 approximation).

simulated recovery, that is, for equilibrium-controlled separations. The accumulation in the intraparticle fluid phase leads to a decrease in the effective adsorption selectivity of the adsorbent, which is attributed to this concentration being normally very close to the concentration in the bulk gas phase.

TM2 approximation, despite being very simple compared to the dusty-gas model, very accurately describes the process performance. This approximation presents the same behavior as the dusty-gas linear driving force approximation, which means that in the range of Ψ studied it is possible to obtain an equivalency between both. There are only slight differences between the TM2 approximation and the homogeneous diffusion equation. This means that a commonly discussed issue of the LDF approximation—wrong response to short cycles—is not problematic for this system in the high product purity region.

Figure 4 shows that the differences between the TM1 and TM2 approximations are not negligible in terms of process performance. Therefore, we decided to study the influence of the particle porosity value on the process performance. Table 4 presents some examples of particle porosities used in simulations involving zeolites of types 5A and 13X, and also the corresponding approximations used to describe the mass transfer.

Figure 5 shows the optimization results considering the TM2 approximation and using different porosity values within the range of published values. From this simple analysis we can see that the value used for porosity in the simulations substantially affects the predictions. The use of accurate values for particle porosities is thus quite important to accurately simulate and optimize cyclic adsorption processes.

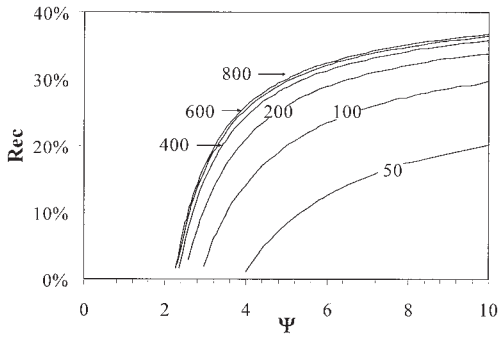

Figure 6. Analysis of the influence of Peclet number (Pe) used in the model.

Maximum recovery as a function of Ψ for a required purity of 95% (O_2 + Ar) and maximum pressure of 5 bar (PSA operation at 20°C).

In addition, the strategy developed here was used to study the influence of the multicomponent adsorption model used on the process simulation (PSA and VSA operation). Several simulations were performed, in the range of pressure and Ψ analyzed in this work, using the IAST model and the multicomponent Langmuir equation for describing the adsorption equilibrium. The results obtained for this system are equivalent to those obtained using the multicomponent Langmuir equation, within an error $< 1\%$.

Analysis of axial dispersion: Peclet number

Once the particle diameter and the column length are known, the Peclet number can be estimated assuming an average molar velocity and a gas mixture composition.[3] Typical values used are around 500 to 1000. In this work we analyze the influence of the Peclet number on the simulated results, shown in Figure 6. They were obtained using the adsorption data of OXYSIV 5 and at a maximum pressure of 5 bar.

From Figure 6, we can conclude that, for Peclet values $>$ 600, the process performance is almost invariant. This is explained by the fact that, above this value, other dispersion effects, such as the gradual column pressurization and the mass transfer resistance, become predominant and the performance becomes insensitive toward axial dispersion effects.

Analysis of pressure ratio

Some issues that are important for the optimization of cyclic adsorption processes were discussed in the previous sections: the mass transport mechanism, the calculation of multicomponent equilibrium, and the dispersive effects. In this section, we turn our focus on determining the optimum operation conditions for oxygen production in both small and large scale. The process performance analysis (in terms of recovery and power consumption) is presented for different pressure ratios, using the Skarstrom cycle, the adsorption data of OXYSIV 5, and maintaining a required purity of 95% (O_2 + Ar).

Figure 7 shows the simulated results (maximum recovery) for different pressure ratios p_T^H/p_T^L for PSA (Figure 7a) and for

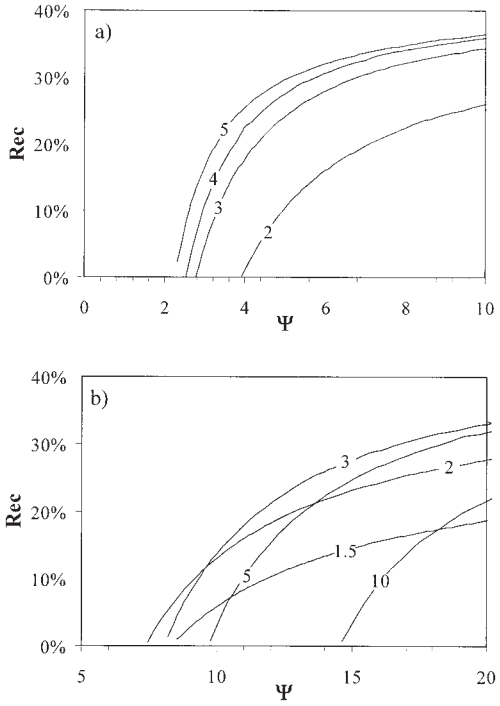

Figure 7. Maximum recovery as a function of Ψ (a) PSA and (b) VSA.

Analysis of different pressure ratios, p_T^H/p_T^L (isothermal operation at 20°C).

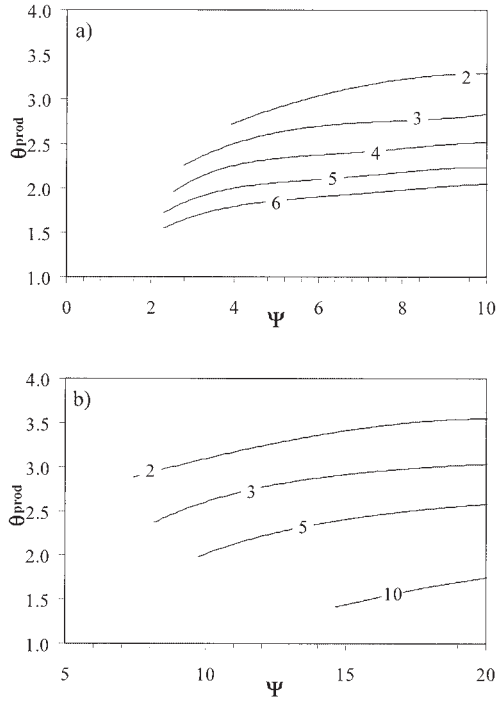

Figure 8. Dimensionless production time (θ_{prod}) as a function of Ψ: (a) PSA and (b) VSA.

Analysis for different pressure ratios, p_T^H/p_T^L (isothermal operation at 20°C).

Table 5. Average Dimensionless Pressurization Time: Analysis for Different Pressure Ratios

PSA		VSA	
p_T^H/p_T^L	θ_{pres}	p_T^H/p_T^L	θ_{pres}
2	0.96 ± 0.08	2	1.01 ± 0.09
3	1.03 ± 0.06	3	1.35 ± 0.07
4	1.21 ± 0.10	5	1.49 ± 0.11
5	1.09 ± 0.07	10	1.50 ± 0.13

VSA (Figure 7b) operation. In PSA, in the pressure range analyzed, the increase of pressure ratio leads to an increase of the maximum recovery. This is more evident, however, at lower pressure ratios as a result of the decrease of adsorption selectivity with pressure (Langmuir-type isotherm).

The maximum recovery in PSA is slightly higher than 35%. In VSA, on the other hand, the increase of pressure ratio does not always lead to an increase in product recovery. For low Ψ values, the recovery is higher for lower pressure ratios; for higher Ψ values, the recovery is higher for higher pressure ratios. In the present case, the maximum recovery is about 30%, which is less than that in PSA (about 5% lower).

Table 5 shows the average of the optimized dimensionless pressurization time for the range of Ψ presented in Figure 7 and the associated error with 95% confidence (assuming a Student's *t*-distribution). The optimal values of the dimensionless pressurization time are practically independent of Ψ. The error for θ_{pres}, under the assumption that it is constant with Ψ , is always <10%. This aspect was also discussed by Cruz et al.,[44] where a constant value of one was assumed in all the optimization results presented.

Figure 8 presents the optimum dimensionless production time, as a function of Ψ, for different pressure ratios. The behavior of this variable for different pressure ratios and as a function of Ψ is analogous for both PSA and VSA operating modes: the dimensionless production time increases with Ψ and decreases with the pressure ratio. The optimum values are between $\theta_{prod} = 1.5$ and $\theta_{prod} = 3.5$.

For high Ψ values, the dimensionless production time is almost constant. This behavior can be very useful in an optimization procedure because it becomes easier to assign an initial guess. Note that, when not using dimensionless variables, the production time depends on the production flow rate, making it difficult to determine a good initial estimate.

Figure 9 shows the optimum normalized purge flow rate χ as a function of Ψ. In PSA, an increase in pressure ratio and in Ψ always leads to a decrease in the normalized purge flow rate. This variable changes considerably for lower values of Ψ, although it is more or less constant for higher Ψ values. As discussed for the dimensionless production time, this behavior is extremely important and can be observed only for dimensionless variables.

Power consumption

This section presents the power consumption of the oxygen production unit for a required purity of 95% (O_2 + Ar) using the Skarstrom cycle for PSA and VSA operating modes.

Figure 10 shows the power consumption as a function of Ψ for different pressure ratios. For high Ψ values, the power consumption always increases with increasing pressure ratio, both for PSA and VSA. For Ψ = 10, the pressure ratio that

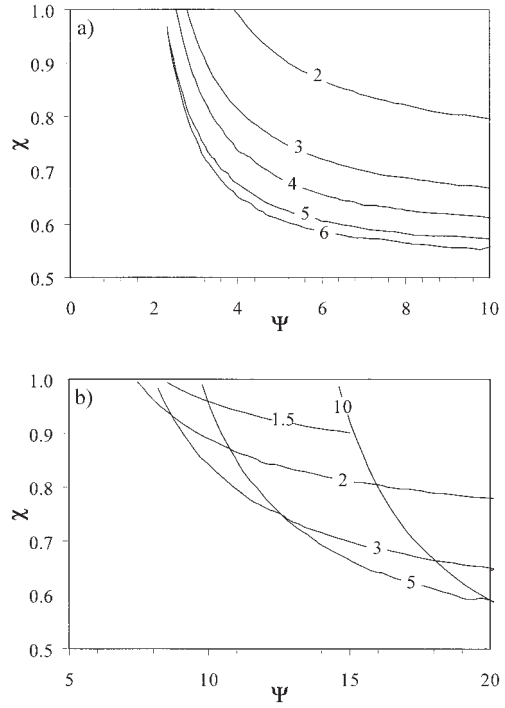

Figure 9. Normalized purge flow rate (χ) as a function of Ψ: (a) PSA and (b) VSA.

Analysis for different pressure ratios, p_T^H/p_T^L (isothermal operation at 20°C).

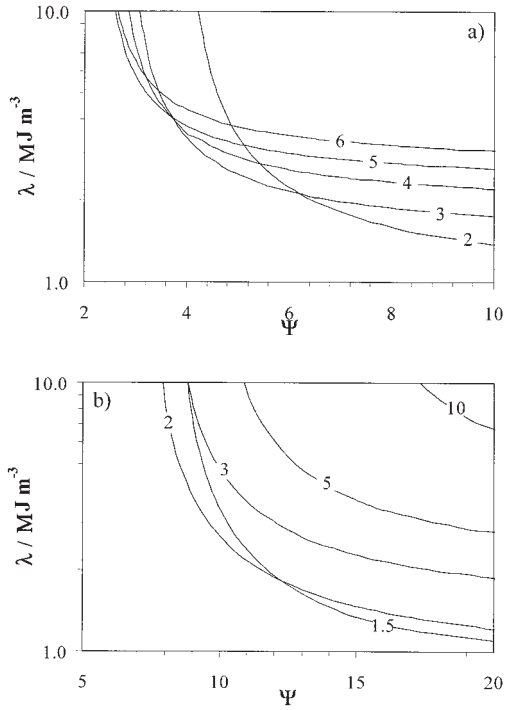

Figure 10. Power consumption as a function of Ψ: (a) PSA and (b) VSA.

Analysis for different pressure ratios, p_T^H/p_T^L (isothermal operation at 20°C).

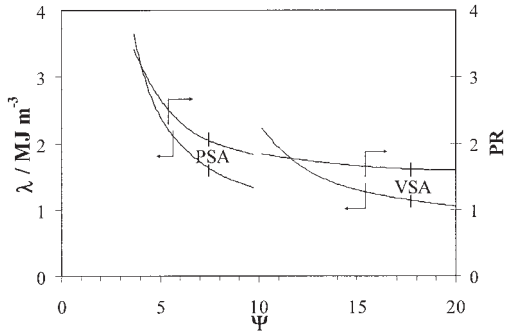

Figure 11. Minimum power consumption and optimum pressure ratio, PR = p_T^H/p_T^L as a function of Ψ (isothermal operation at 20°C).

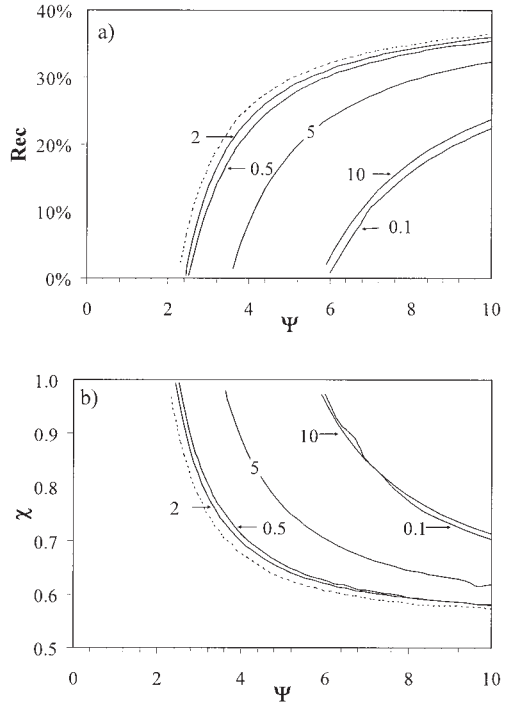

Figure 12. (a) Maximum recovery and (b) normalized purge flow rate (χ) as a function of Ψ.

—, different values of dimensionless pressurization time (θ_{pres}) and - - -, optimum value of dimensionless pressurization time (PSA operation at 20°C).

minimizes the power consumption for PSA is about 2 bar. However, for $\Psi = 4$ it is about 3 bar and, for lower values of Ψ, the corresponding pressure ratio increases significantly. For the VSA operating mode, the purge pressure that minimizes the power consumption is always >500 mbar (pressure ratio = 2).

Figure 11 shows the minimum power consumption as a function of Ψ (results obtained by minimizing the power consumption). As can be observed, the pressure that minimizes the power consumption for VSA is about 600 mbar (pressure ratio $\cong$ 1.7). In PSA, the optimum operating pressure decreases with increasing Ψ. In both cases, it is verified that the power consumption varies inversely with Ψ. In dimensional variables, the decrease of Ψ implies the decrease of the column dimensions and/or the increase of the product flow rate.

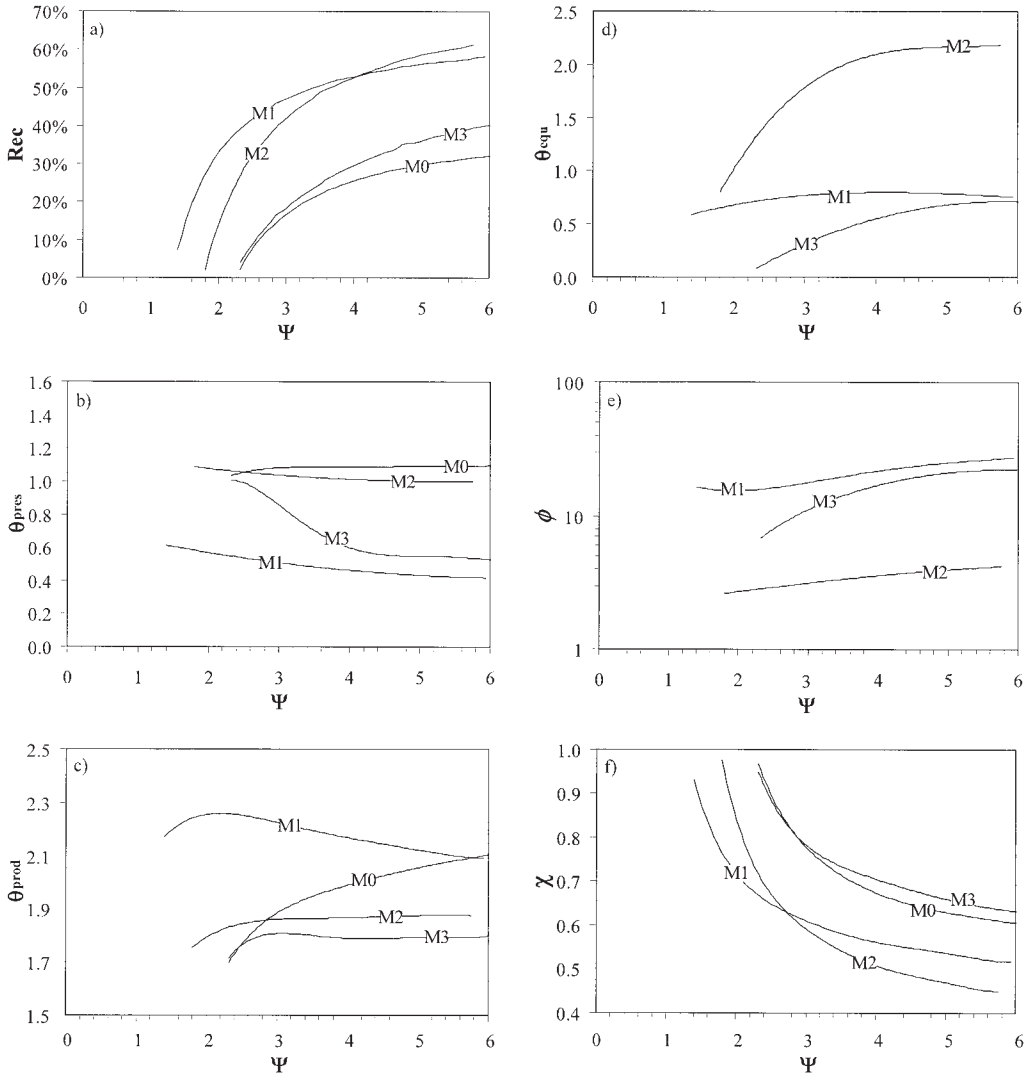

Figure 13. Optimization results for a PSA cycle with equalization stage and for $p_T^H = 5$ bar.

(a) Maximum recovery, (b) dimensionless pressurization time (θ_{pres}), (c) dimensionless production time (θ_{prod}), (d) dimensionless equalization time (θ_{equ}), (e) dimensionless valve coefficient (ϕ), and (f) normalized purge flow rate (χ) as a function of Ψ.

Influence of dimensionless pressurization time

From the analysis of Table 5 we verify that the dimensionless pressurization time has a practically negligible influence on the process performance. To clarify this issue, only two decision variables were considered in the process optimization: the dimensionless production time (θ_{prod}) and the normalized purge flow rate (χ). A dimensionless pressurization time (θ_{pres}) equal to one was considered in the optimization. The simulated results confirm what was suspected: making the dimensionless pressurization time equal to one is a good guess in the range of Ψ and pressure ratios analyzed. To conclude this analysis, Figure 12 shows the optimization results for different values of dimensionless pressurization time for a maximum pressure of 5 bar (for PSA operation).

One can observe two interesting aspects in Figure 12: first, the influence of dimensionless pressurization time (θ_{pres}) in the process performance dramatically decreases with the increase of Ψ; second, its influence in the process follows a logarithmic form and so, to optimize the process efficiently, it is convenient to analyze θ_{pres} in a logarithmic scale. This was done for the simulations presented here.

Figure 12 shows that the influence of dimensionless pressurization time in the process performance is practically negligible in a range of θ_{pres} around unity. However, an optimum value can be found and the process performance can be dramatically reduced if a value is assigned without performing a prior study for the system in question.

Analysis of cycle configuration

This section presents the study of the three configurations presented for the Skarstrom cycle with equalization. The process performance is analyzed in terms of recovery. The results were obtained using the adsorption data for the OXYSIV 5. Figure 13 presents the optimization results for the PSA operation mode and for a maximum pressure of 5 bar.

Configuration M3 (bottom to bottom) is apparently more efficient than the Skarstrom cycle without equalization (configuration M0) only for high Ψ values. For lower Ψ values, M3

performance tends to the Skarstrom cycle without equalization, attributed to the equalization flow rate becoming almost zero (very low dimensionless equalization time). The equalization flow rate taken from the column base has a composition that is less rich in oxygen than the feed mixture. For this reason, when using configuration M3 for high Ψ values, the dimensionless production time is lower than the corresponding values using the Skarstrom cycle, whereas the normalized purge flow is higher.

Configurations M1 (top to bottom) and M2 (top to top) are substantially more efficient, although they are marked by the inconvenience of implying the implementation of more electric valves. These configurations are extremely attractive for large-scale production, where power consumption is the main issue. However, their implementation in small-scale production must be decided with care because of the increase of system complexity. For small-scale production, configuration M3 can be implemented in the same way as the Skarstrom cycle without equalization.

Configuration M1 is favored by an equalization stage with a low equalization time (higher flow rate) compared with configuration M2: for configuration M1, $\theta_{equ} \cong 0.5$ (dimensionless equalization time) and $\phi = 20$ (dimensionless coefficient of the equalization valve), whereas for configuration M2, $\theta_{equ} \cong 2$ (for higher Ψ values) and $\phi \cong 4$.

In configuration M1, the equalization flow comes from the base and displaces the gas in the column toward the top of the other column. In configuration M2, the equalization flow comes from the top and displaces the gas down to the column base. In this last configuration, the gas composition in the column's top is always richer in product when a new cycle began, resulting from the gas stream that comes from the other column. As a direct consequence, the normalized purge flow rate substantially decreases, thus increasing the recovery.

Several simulations were performed for different operating pressures. The results obtained follow the same tendency as presented before: configuration M3 (bottom to bottom) is more efficient than M0 (the Skarstrom cycle without equalization) only for high Ψ values and configuration M2 (top to top) is the overall optimal configuration.

Oxygen Production from Air: Adsorbent OXYSIV 7

The optimization results for the oxygen production unit using the adsorption data of OXYSIV 7 are presented and discussed in this section.

Analysis of pressure ratio

This section analyzes the effect of the pressure ratio on the process performance (recovery and power consumption), considering the adsorption data of OXYSIV 7 and the Skarstrom cycle without equalization.

For the PSA operation mode (Figure 14) the increase of maximum pressure always leads to an increase in the maximum recovery. The data presented before for OXYSIV 5 indicated that an increase in pressure ratio > 5 bar leads to an insignificant increase in the maximum recovery. With the adsorption data of OXYSIV 7 it can be seen that this limiting pressure can be assumed to be 3 bar (considering the improvement in relative values). This fact can be understood from the analysis of the nitrogen adsorption isotherm in both adsorbents. This isotherm is more favorable (stronger curvature) in the case of OXYSIV 7, thus presenting higher selectivities at low pressures.

For operation with this adsorbent, as in the case of OXYSIV 5, the increase in the pressure ratio leads to a decrease in the dimensionless production time and to an increase in the normalized purge flow, arising from the decrease in adsorption selectivity. The power consumption, compared with that of OXYSIV 5, is drastically reduced.

In the VSA operation mode (Figure 15), as in PSA, increasing pressure ratio leads to an increase in the maximum recovery. In the case of OXYSIV 5, the results were somewhat different, showing different behaviors for high and low values of Ψ. The operation in VSA, compared with that in PSA, for the same project characteristics, is more economical with respect to power consumption. This adsorbent type is normally recommended for PSA operation using a low pressure ratio and for VSA operation.

As in the case of OXYSIV 5, the strategy developed was used to study the sensitivity of the simulations to the multicomponent adsorption model used. For that, several simulations were made using IAST. The results obtained using both models are now significantly different. Actually, the Langmuir–Freundlich equation leads to more conservative optimization results (lower recoveries). This seems to be an important aspect that should be taken in account to obtain more precise results. Future work should consider experimental determination of multicomponent adsorption data.

Conclusions

Simulation tools and an optimization strategy for the optimization of cyclic adsorption processes were developed in this work, using efficient numeric techniques elaborated within our group.[44-46] Stability and accuracy of the simulation results were simultaneously ensured. The optimization strategy was tested for oxygen production from air, using adsorption data for two commercially available adsorbents.

The simulator assumes perfect gas behavior, uniform cross-sectional void fraction, uniform adsorbent properties along the column, negligible radial gradients, and isothermal behavior. Five different approximations were considered for describing the mass transport within the particle.

(1) Linear driving force approximation, assuming negligible accumulation in the intraparticle gas phase (TM1).

(2) Linear driving force approximation, assuming instantaneous equilibrium between the interparticle gas phase and the intraparticle gas phase (TM2).

(3) Linear driving force dusty-gas model (TM3).

(4) Homogeneous mass diffusion equation, assuming instantaneous equilibrium between the interparticle gas phase and the intraparticle gas phase (TM4).

(5) The dusty-gas model (TM5).

In the simulator, the adsorption equilibrium is described using the Langmuir and Langmuir–Freundlich multicomponent equations and the ideal adsorbed solution theory (IAST).

The proposed optimization strategy considers the problem in a dimensionless form. In this way, the mathematical equations that describe the system do not depend on the actual unit scale or on primary variables (such as product flow rate, pressurization time, and production time), but on dimensionless vari-

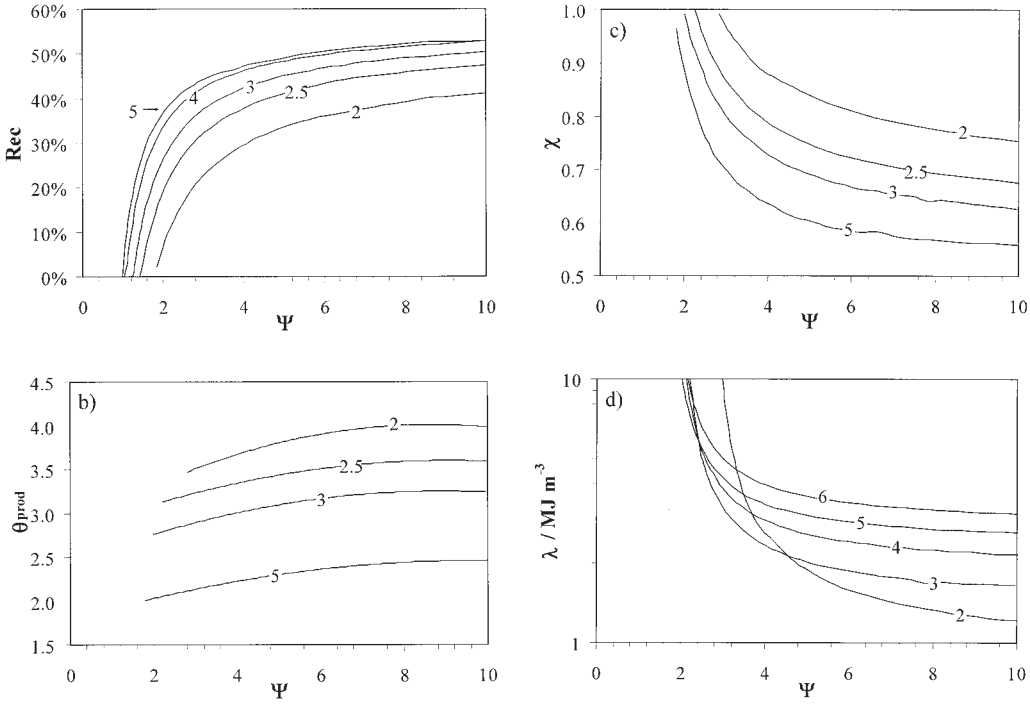

Figure 14. Optimization results.

(a) Maximum recovery, (b) dimensionless production time (θ_{prod}), (c) normalized purge flow rate (χ), and (d) power consumption as a function of Ψ for PSA operating mode at 20°C. Analysis at different pressure ratios, p_T^H/p_T^L.

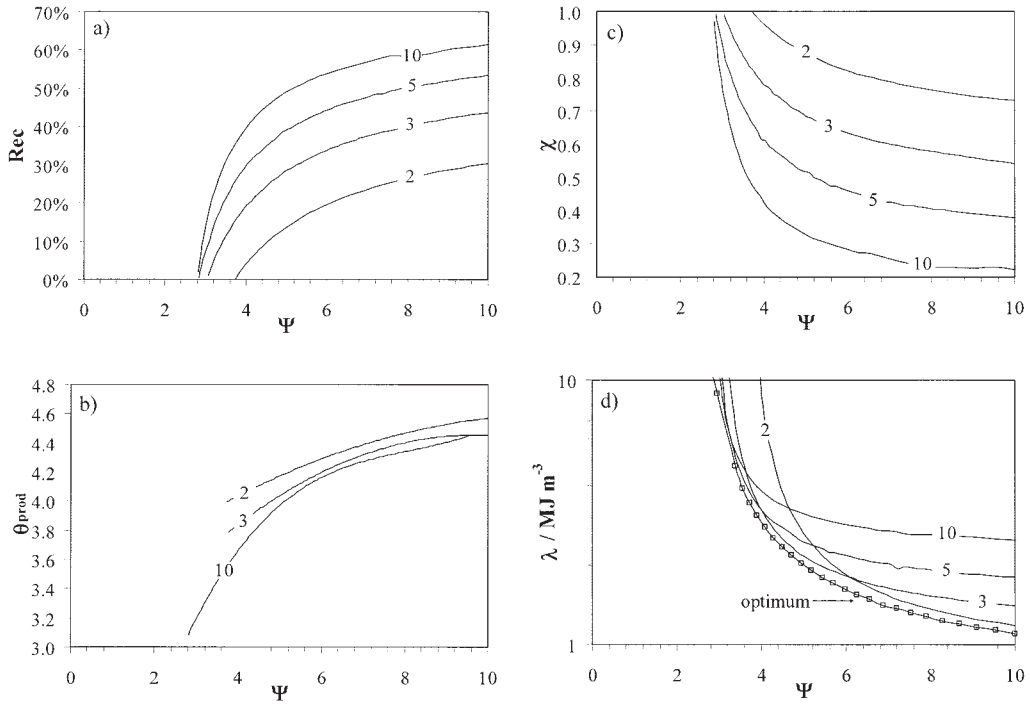

Figure 15. Optimization results.

(a) Maximum recovery, (b) dimensionless production time (θ_{prod}), (c) normalized purge flow rate (χ), and (d) power consumption as a function of Ψ in VSA. Analysis at different pressure ratios, p_T^H/p_T^L.

ables, which are to be optimized. The reference variables were selected to make the optimization algorithm as efficient as possible. A successive quadratic-programming algorithm (SQP) was developed, which proved to be very efficient and robust in the optimization of this kind of problems that are intrinsically dynamic.

The proposed approach proved to be useful not only for characterizing the process performance (in terms of recovery and power consumption) for the two adsorbents, but also in the study of different configurations for the equalization stage. This approach was also useful in the study of the influence of different operation and project variables.

When considering the different mass transport approximations in the simulator, we conclude that the linear driving force, assuming instantaneous equilibrium between the interparticular gas phase and the intraparticular gas phase (TM2), satisfactorily describes the systems under study (oxygen separation from air). This approximation yielded results that are very close to the homogeneous diffusion equation and the dusty-gas model. The particle porosity value used in the simulations significantly influences the results obtained. Published porosity values vary between 0 and 0.65, which can lead to differences of about 10% in maximum recovery.

The axial dispersion in the bed, translated by the Peclet number, proves to be almost negligible for Peclet numbers > 600. The use of a constant Peclet number was adopted in this work.

For oxygen production from air using adsorbent OXYSIV 7 UOP™, the results obtained using the multicomponent Langmuir–Freundlich equation for describing adsorption equilibrium are significantly different from the results using the IAST. Future work should consider the experimental determination of multicomponent data to obtain better simulation results.

For the considered gas separation units and for isothermal operating conditions, the increase of pressure ratio always leads to an improvement in process performance. The best performance (in terms of recovery and power consumption) for oxygen production from air using the adsorbent OXYSIV 5 UOP™ is for PSA operation mode. In the case of OXYSIV 7, the best performance is for VSA.

For oxygen production from air using adsorbent OXYSIV 5, the dimensionless production time (θ_{prod}) and the normalized purge flow rate (χ) are the most important decision variables. The optimum dimensionless pressurization time (θ_{pres}) can, in this case, be assumed to be invariant with pressure ratio and adsorbent productivity, without implying any significant inaccuracy in the optimization results.

The study of the equalization stage configuration showed that the bottom-to-bottom configuration (M3) is more efficient than the Skarstrom cycle only for low values of adsorbent productivity. The top-to-top configuration (M2) proves to be, in all the analyzed cases, the most efficient configuration in terms of recovery and power consumption.

Future work in this area should be directed to an enlarged study of processes in nonisothermal conditions and of more complex processes involving multiple beds, for instance. Initially classic cycles, such as those developed by Wagner,[21] Batta,[65] and McCombs[66] can be considered. These cycles are very often used in practice but rarely studied theoretically, using simulation approaches.

Acknowledgments

The work of Paulo Cruz was supported by FCT Grant BD/21483/99 and POSI/SFRH/BPD/13539/2003. The research was also supported by funds from FCT project POCTI/EQU/380672001.

Notation

$\mathbf{B}$ = diffusivity matrix in dusty-gas model, m^2/s
b_i = Langmuir affinity constant, 1/bar
c = fluid phase molar concentration, mol/m^3
D_{ax} = effective axial dispersion coefficient, m^2/s
$D^e_{M,i}$ = effective homogeneous diffusion coefficient, m/s
d = diameter, m
k = iteration or LDF coefficient, $k_i = 15D^e_{M,i}/r_p^2$, 1/s
L = length column, m
N = molar flow rate, $mol\ m^{-3}\ s^{-1}$
$\mathbf{N}^p$ = flux in the void space, $mol\ m^{-3}\ s^{-1}$
$\mathbf{N}^s$ = fluxes in the adsorbed phase, $mol\ m^{-3}\ s^{-1}$
nc = number of mixture components
p = pressure, Pa
Pe = Peclet number, $Pe = u_{ref}L/D_{ax}$
Pur = product purity, %
q = molar concentration in the adsorbed phase, mol/m^3
q_{max} = isotherm parameter, maximum capacity, mol/kg
r = radius, m
$\Re$ = universal gas constant, $J\ mol^{-1}\ K^{-1}$
R = dimensionless radial coordinate
Rec = product recovery
t = time variable, s
u = average interstitial molar velocity, m/s
x = dimensionless spatial coordinate, $x = z/L$
y = gas phase molar fraction
z = spatial coordinate, m

Greek letters

α = dimensionless d'Arcy parameter, $\alpha = [150\mu_{mix}(1 - \varepsilon_b)^2 u_{ref}L]/\varepsilon_b^3 d_p^2 p_{ref}$
α^M = ratio between diffusivity coefficients, $\alpha_i^M = D^e_{M,i}/D_{ref} = k_i/k_{ref}$
ζ_a = adsorbed phase capacity factor, $\zeta_a = (1 - \varepsilon_p)[(1 - \varepsilon_b)/\varepsilon_b](q_{ref}/c_{ref})$
ζ_p = fluid phase capacity factor, $\zeta_p = (1 - \varepsilon_b)/\varepsilon_b\varepsilon_p$
θ = dimensionless time variable, $\theta = t/\tau_b$
τ_b = bed time constant, $\tau_b = L/u_{ref}$
λ = power consumption, MJ/m^3
Ψ = optimization parameter, $\Psi = \varphi[(\theta_{prod} + \theta_{pres} + \theta_{equ})/\theta_{prod}](p_T^0/p_T^H)(T/T^0)$
χ = normalized purge velocity, $\chi = (u_{purg}/u_{ref})(p_T^L/p_T^H)$
ε_b = bed porosity (ratio between the free volume and the total volume)
ε_p = particle porosity
μ_{mix} = mixture viscosity, $kg\ m^{-1}\ s^{-1}$
φ = ratio between bed time constant and particle diffusion time constant (LDF approximation), $\varphi = \tau_b k_{ref}$ $(=15\Phi)$
Φ = ratio between bed time constant and particle diffusion time constant (homogeneous diffusion equation), $\Phi = \tau_b D_{ref}/r_p^2$
ρ_s = apparent particle density, kg/m^3
ϕ = dimensionless coefficient of the equalization valve
Ω = adsorbent productivity, $m^3_{STP}\ year^{-1}\ m^{-3}$

Subscripts

equ = equalization
i = component
pres = pressurization
prod = production
purg = purge
ref = reference
T = total

Superscripts

* = dimensionless variable
L = low
H = high

Literature Cited

1. Sherman JD. Synthetic zeolites and other microporous oxide molecular sieves. *Proc Natl Acad Sci USA*. 1999;96:3471-3478.
2. Khale H. Adsorptionsverfahren. DE Patent No. 871 886; 1942.

3. Ruthven DM. *Principles of Adsorption and Adsorption Processes*. New York, NY: Wiley; 1984.
4. Yang RT. *Gas Separation by Adsorption Processes*. Boston, MA: Butterworths; 1987.
5. Ruthven DM, Farooq S, Knaebel KS. *Pressure Swing Adsorption*. New York, NY: VCH Publishers; 1994.
6. Skarstrom CW. Method and apparatus for fractionating gaseous mixtures by adsorption. U.S. Patent No. 2 944 627; 1960.
7. Montgareuil PG, Domine D. Process for separating a binary gas mixture by adsorption. U.S. Patent No. 3 155 468; 1964.
8. Milton RM. Molecular sieve adsorbents. U.S. Patent No. 2 992 243; 1959.
9. Milton RM. Molecular sieve adsorbents. U.S. Patent No. 2 992 244; 1959.
10. Coe CG, Kuznicki SM. Polyvalent ion exchanged adsorbent for air separation. U.S. Patent No. 4 481 018; 1984.
11. Chao CC. Process for separating nitrogen from mixtures thereof with less polar substances. U.S. Patent No. 4 859 217; 1989.
12. Chao CC, Sherman JD, Mullhaupt JT, Bolinger C. Mixed ion-exchanged zeolites and processes for the use thereof in gas separations. U.S. Patent No. 5 174 979; 1992.
13. Coe CG, MacDougall JE, Weigel SJ. Magnesium A-zeolite for nitrogen adsorption. U.S. Patent No. 5 354 360; 1994.
14. Hess B, Puppe L, Reiss G. Binder-free molecular sieve zeolite granules which contain zeolites of the type lithium zeolite A and lithium zeolite X. U.S. Patent No. 5 962 358; 1999.
15. Hess B, Puppe L, Reiss G. Binder-free molecular sieve zeolite granules which contain zeolites of the type lithium zeolite A and lithium zeolite X. U.S. Patent No. 6 051 051; 2000.
16. Li YY, Perera SP, Crittenden BD, Bridgwater J. The effect of the binder on the manufacture of 5A zeolite monolith. *Powder Technol.* 2001;116:85-96.
17. Hill CC, Hill TB. Fluid fractionator. U.S. Patent No. 5 730 778; 1998.
18. Hill TB, Hill CC, Hansen AC. Rotary valve assembly for pressure swing adsorption system. U.S. Patent No. 6 311 719; 2001.
19. Marsh WD, Pramuk FS, Hoke RC, Skarstrom CW. Pressure equalization depressurising in heatless adsorption. U.S. Patent No. 3 142 547; 1964.
20. Berlin NH. Method for providing an oxygen-enriched environment. U.S. Patent No. 3 280 536; 1966.
21. Wagner JL. Selective adsorption process. U.S. Patent No. 3 430 418; 1969.
22. Warmuzinski K. Effect of pressure equalization on power requirements in PSA systems. *Chem Eng Sci.* 2002;57:1475-1478.
23. Fuderer A, Rudelstorfer E. Selective adsorption process. U.S. Patent No. 3 846 849; 1976.
24. Malek A, Farooq S. Study of a six-bed pressure swing adsorption process. *AIChE J.* 1997;43:2509-2523.
25. Malek A, Farooq S. Hydrogen purification from refinery fuel gas by pressure swing adsorption. *AIChE J.* 1998;44:1985-1992.
26. Sircar S, Golden TC. Purification of hydrogen by pressure swing adsorption. *Sep Sci Technol.* 2000;35:667-687.
27. Chiang AST, Chung YL, Chen CW, Hung TH, Lee TY. Experimental study on a four-bed PSA air separation process. *AIChE J.* 1994;40: 1976-1982.
28. Farooq S, Ruthven DM. Numerical simulation of a kinetically controlled pressure swing adsorption bulk separation process based on a diffusion model. *Chem Eng Sci.* 1991;46:2213-2224.
29. Lee CH, Yang J, Ahn H. Effects of carbon-to-zeolite ratio on layered bed H2 PSA for coke oven gas. *AIChE J.* 1999;45:535-545.
30. Warmuzinski K, Tanczyk M. Multicomponent pressure swing adsorption Part I. Modelling of large-scale PSA installations. *Chem Eng Process.* 1997;36:89-99.
31. Bhaumik S, Majumdar S, Sirkar KK. Hollow-fiber membrane-based rapid pressure swing adsorption. *AIChE J.* 1996;72:409-421.
32. Stoner G, Reingold HE, D'Amico JS, Knaebel KS. Enhanced helium recovery. U.S. Patent No. 5 632 803; 1997.
33. Prasad R, Cook PJ, Gottzman CF. Air separation system and method. U.S. Patent No. 5 827 351; 1998.
34. Feng X, Pan CY, Ivory J, Ghosh D. Integrated membrane/adsorption process for gas separation. *Chem Eng Sci.* 1998;53:1689-1698.
35. Sirkar KK. Method and apparatus for gas removal by cyclic flow swing membrane permeation. U.S. Patent No. 5 928 409; 1999.
36. Ruthven DM, Farooq S. Air separation by pressure swing adsorption. *Gas Sep Purif.* 1990;4:141-148.
37. Farooq S, Ruthven DM, Boniface HA. Numerical simulation of pressure swing adsorption oxygen unit. *Chem Eng Sci.* 1989;44:2809-2816.
38. Mendes AMM, Costa CAV, Rodrigues AE. Analysis of nonisobaric steps in nonlinear bicomponent pressure swing adsorption systems. Application to air separation. *Ind Eng Chem Res.* 2000;39:138-145.
39. Mendes AMM, Costa CAV, Rodrigues AE. Oxygen separation from air by PSA: Modelling and experimental results. Part I: Isothermal operation. *Sep Purif Technol.* 2001;24:173-188.
40. Smith OJ, Westerberg AW. The optimal design of pressure swing adsorption systems. *Chem Eng Sci.* 1991;46:2967-2976.
41. Nilchan SE, Pantelides CC. On the optimization of periodic adsorption processes. *Adsorption.* 1998;4:113-147.
42. Ding Y, Croft DT, LeVan MD. Periodic states of adsorption cycles: IV. Direct optimization. *Chem Eng Sci.* 2002;57:4521-4531.
43. Jiang L, Biegler L, Fox V. Simulation and optimization of pressure swing adsorption systems for air separation. *AIChE J.* 2003;49:1140-1157.
44. Cruz P, Santos JC, Magalhães FD, Mendes A. Cyclic adsorption separation processes: Analysis strategy and optimization procedure. *Chem Eng Sci.* 2003;58:3143-3158.
45. Cruz P, Alves MA, Magalhães FD, Mendes A. Solution of hyperbolic PDEs using a stable adaptive multiresolution method. *Chem Eng Sci.* 2003;58:1777-1792.
46. Cruz P, Magalhães FD, Mendes A. High-order approximations for adsorption in a particle. *Chem Eng Sci.* 2004;59:4393-4399.
47. Glueckauf E. Theory of chromatography. Part 10: Formula for diffusion into spheres and their application to chromatography. *Trans Faraday Soc.* 1955;51:1540-1551.
48. Liaw C, Wang J, Greenkorn R, Chao K. Kinetics of fixed bed adsorption studies—New solution. *AIChE J.* 1979;25:376-381.
49. Do DD. *Adsorption Analysis: Equilibria and Kinetics*. London: Imperial College Press; 1998.
50. Lee J, Kim DH. High-order approximations for noncyclic and cyclic adsorption in a particle. *Chem Eng Sci.* 1998;53:1209-1221.
51. Chou CT, Huang WC. Incorporation of a valve equation into the simulation of a pressure swing adsorption. *Chem Eng Sci.* 1994;49: 75-84.
52. Chou CT, Huang WC. Simulation of a four-bed pressure swing adsorption process for oxygen enrichment. *Ind Eng Chem Res.* 1994;33: 1250-1258.
53. Myers AL, Prausnitz JM. Thermodynamics of mixed gas adsorption. *AIChE J.* 1965;11:121-127.
54. Petzold LR. Automatic selection of methods for solving stiff and nonstiff systems of ordinary differential equations. *SIAM J Sci Stat Comput.* 1983;4:136-148.
55. Harten A. High resolution schemes for hyperbolic conservation laws. *J Comput Phys.* 1983;49:357-393.
56. Sweby PK. High resolution schemes using flux limiters for hyperbolic conservation laws. *SIAM J Numer Anal.* 1984;21:995-1011.
57. Leonard BP. Locally modified QUICK scheme for highly convective 2-D and 3-D flows. In: Taylor C and Morgan K, eds. *Numerical Methods in Laminar and Turbulent Flow* (Vol. 5). Swansea, UK: Pineridge Press; 1987:35-47.
58. Darwish MS, Moukalled F. Normalized variable and space formulation methodology for high-resolution schemes. *Num Heat Transfer B.* 1994;26:79-96.
59. Gaskell PH, Lau AKC. Curvature compensated convective transport: SMART. A new boundedness preserving transport algorithm. *Int J Numer Meth Fluids.* 1988;8:617-641.
60. Alves MA, Oliveira PJ, Pinho FT. A convergent and universally bounded interpolation scheme for treatment of advection. *Int J Numer Meth Fluids.* 2003;41:47-75.
61. Peters MS, Timmerhaus KD. *Plant Design and Economics for Chemical Engineers*. New York, NY: McGraw-Hill; 1980.
62. Edgar TF, Himmelblau DM. Optimization of chemical processes. Mexico City, Mexico: Libros McGraw-Hill de Mexico; 1988.
63. Gales L, Mendes A, Costa C. Hysteresis in the cyclic adsorption of acetone, ethanol and ethyl acetate on activated carbon. *Carbon.* 2000; 38:1083-1088.
64. Keller JU, Dreisbach F, Rave H, Staudt R, Tomalla M. Measurement

of gas mixture adsorption equilibria of natural gas compounds on microporous sorbents. *Adsorption.* 1999;5:199-214.
65. Batta LB. Selective adsorption gas separation process. U.S. Patent No. 3 636 679; 1972.
66. McCombs NR. Selective adsorption gas separation process. U.S. Patent No. 3 738 087; 1973.

Appendix: Successive Quadratic-Programming Algorithm

A successive quadratic-programming algorithm approximates the objective function locally by a quadratic function, and the constraint by linear functions, so that quadratic programming could be used recursively.[62] The optimal solution obtained satisfies the necessary Kuhn–Tucker conditions. In our algorithm the variable bounds are treated as general inequality constraints and we use the so-called equality-constrained version (EQP)[62] for the treatment of inequality constraints, that is, the inequality constraints that are members of the active set become equality constraints. The algorithm is described by the following steps:

(1) Initialization

Let $k = 0$.

Pick $\mathbf{r}^k$, $\mathbf{x}^k$, $\mathbf{B}^k$ ($\mathbf{B}^k = \mathbf{I}$)

where $\mathbf{x}$ is the vector of decision variables, $\mathbf{B}$ is an estimative of the Hessian matrix, and $\mathbf{r}$ is the weighting coefficient of penalty function.

(2) Calculate members of active set of constraints (all the equality constraints plus the active inequality constraints): that is, $h_j(\mathbf{x}^k) = \mathrm{Pur}_R - \mathrm{Pur}$

Calculate the objective function value, $f(\mathbf{x}_k)$

Calculate the gradients $\nabla\mathbf{f}(\mathbf{x}^k)$ and $\nabla\mathbf{h}(\mathbf{x}^k)$

(3) Estimate the Lagrange multiplier, $\mathbf{u}^k$

$$\mathbf{u}^k = [\nabla\mathbf{h}^k \cdot (\mathbf{B}^k)^{-1} \cdot (\nabla\mathbf{h}^k)^T]^{-1} \cdot [\nabla\mathbf{h}^k \cdot (\mathbf{B}^k)^{-1}\nabla\mathbf{f}^k - \mathbf{h}^k]$$

(4) Calculate the new search direction, $\mathbf{s}^k$

$$\mathbf{s}^k = (\mathbf{B}^k)^{-1}[(\nabla\mathbf{h}^k)^T \cdot \mathbf{u}^k - \nabla\mathbf{f}^k]$$

(5) Calculate the weighting coefficient of penalty function, $\mathbf{r}$

$$\mathbf{r} = \max[|\mathbf{u}|, 0.5(|\mathbf{u}| + \mathbf{r})]$$

(6) Calculate the step length λ^k and the new $\mathbf{x}$

(6.1) $\lambda^k = 1$; $i = 0$

(6.2) Calculate $\mathbf{x}^* = \min[\max(\mathbf{x}^k + \lambda^k \cdot \mathbf{s}^k, \mathbf{x}_L), \mathbf{x}_H]$, where $\mathbf{x}_L$ is the lower bound and $\mathbf{x}_H$ is the higher bound of the variables.

(6.3) Calculate members of active set of constraints (all the equality constraints plus the active inequality constraints): that is, $h_j(\mathbf{x}^*) = \min(0, \mathrm{Pur}_R - \mathrm{Pur})$

(6.4) Calculate the objective function value, $f(\mathbf{x}^*)$

(6.5) If $\{f(\mathbf{x}^*) - f(\mathbf{x}^k) + \sum r_j[|h_j(\mathbf{x}^*)| - |h_j(\mathbf{x}^k)|]\} > 0$, Then

Set $\lambda^k = \lambda^k/2^i$; Set $i = i + 1$; Go to Step (6.2)

Else

$\mathbf{x}^{k+1} = \mathbf{x}^*$; Go to Step (7)

(7) Calculate the gradients $\nabla\mathbf{f}(\mathbf{x}^{k+1})$ and $\nabla\mathbf{h}(\mathbf{x}^{k+1})$

(8) New estimate of the Hessian matrix, $\mathbf{B}$, by BFGS method[62]:

$$\mathbf{B}^{k+1} = \mathbf{B}^k + \frac{\Delta\mathbf{g}^k(\Delta\mathbf{g}^k)^T}{(\Delta\mathbf{g}^k)^T\Delta\mathbf{x}^k} - \frac{\mathbf{B}^k\Delta\mathbf{x}^k(\Delta\mathbf{x}^k)^T\mathbf{B}^k}{(\Delta\mathbf{x}^k)^T\mathbf{B}^k\Delta\mathbf{x}^k}$$

where $\Delta\mathbf{g}^k = \nabla_{\mathbf{x}}L(\mathbf{x}^{k+1}, \mathbf{u}^{k+1}) - \nabla_{\mathbf{x}}L(\mathbf{x}^k, \mathbf{u}^{k+1})$, $\Delta\mathbf{x} = \mathbf{x}^{k+1} - \mathbf{x}^k$ and L is the Lagrange function, given by $L(\mathbf{x}, u) = f(\mathbf{x}) - \sum u_j h_j(\mathbf{x})$

(9) Termination

Termination criteria used:

$$\frac{\|x^k - x^{k-1}\|}{\|x^k\| + 1} \le \varepsilon_R \qquad \|x^k - x^{k-1}\| \le \varepsilon_A \qquad \text{and}$$

$$|h(\mathbf{x}^k)| \le \varepsilon_A$$

where ε_R is the relative tolerance and ε_A is the absolute tolerance.

If all the criteria are satisfied, Stop

Otherwise, Continue.

(10) Set $k = k + 1$, go to Step (3).

Manuscript received Aug. 31, 2003, and revision received Aug. 31, 2004.